Applied Catalysis B: Environmental 301 (2022) 120786

Contents lists available at ScienceDirect

Applied Catalysis B: Environmental

journal homepage: www.elsevier.com/locate/apcatb

Heterogeneous catalytic ozonation and peroxone-mediated removal of Acetaminophen using natural and modified hematite-rich soil, as efficient and environmentally friendly catalysts

Mona Kohantorabi [a], Gholamreza Moussavi [a,*], Paula Oulego [b], Stefanos Giannakis [c]

[a] Department of Environmental Health Engineering, Faculty of Medical Sciences, Tarbiat Modares University, Tehran, Iran
[b] Department of Chemical and Environmental Engineering, University of Oviedo, C/ Julián Clavería s/n., Oviedo, E-33071, Spain
[c] Universidad Politécnica de Madrid, E.T.S. Ingenieros de Caminos, Canales y Puertos, Departamento de Ingeniería Civil: Hidráulica, Energía y Medio Ambiente, Unidad docente Ingeniería Sanitaria, c/ Profesor Aranguren, s/n, ES-28040 Madrid, Spain

ARTICLE INFO

Keywords:
Catalytic ozonation
Peroxone
Natural iron
α-Fe_2O_3 structure
Acetaminophen oxidation

ABSTRACT

Hormuz Red Soil (HRS), as a naturally hematite-containing mineral was used to enhance the catalytic ozonation process (COP) of Acetaminophen (ACT) elimination. The surface properties and particle size of HRS mainly composed of *α*-Fe_2O_3 were modified via calcination (C-HRS) demonstrating notable catalytic activity. The catalytic activity of C-HRS was evaluated for the ozonation of ACT under various conditions. Complete degradation of 50 mg L^{-1} ACT was obtained within 10 min at natural conditions with 1.0 g L^{-1} of C-HRS which was > 10 times faster than single ozonation process (SOP). The C-HRS accelerated the decomposition of ozone to hydroxyl radical on the catalyst's surface. Moreover, the C-HRS efficiently catalyzed the peroxone reaction for the degradation and mineralization of ACT. The C-HRS exhibited high stability and reusability in consecutive catalytic cycles. This work offers a new, effective, and low-cost catalyst for accelerating of ozone decomposition that can be used in oxidation of pollutants.

1. Introduction

In the last decade, one of the most important issues considered by Environmental Engineers was related to water pollution, including heavy metals, and (in)organic pollutants, which are released to water through various industries [1,2] or human use [2]. Among the recalcitrant organic contaminants of anthropogenic origin, Acetaminophen (ACT) is the most popular antipyretic pharmaceutical, widely used around the world, and in some countries without any medical prescription [3]. Due to the presence of this compound in the wastewater of hospitals, pharmaceutical manufacturing companies, and urban areas, it is important to develop efficient methods for the removal of this persistent compound from the environment [4]. Different technologies including adsorption [5], advanced oxidation process (AOPs) such as photocatalysis [6], electro-Fenton [7], photo-Fenton [8], and catalytic ozonation [9] were so far applied for the removal and degradation of ACT before discharge in the environment.

Among the aforementioned methods, catalytic ozonation process was developed as a promising method for the wastewater disinfection and removal of organic pollutants in industrial-scale, due to its high activity, strong oxidation ability, and high mineralization rate of pollutants [10]. Ozone (O_3) gas, with its high oxidizing potential (E^0 = 2.08 *V*) is widely used in industrial wastewater treatment for the removal of organic and inorganic compounds [11]. In this process, the reactive species, especially hydroxyl radical ($HO^{\bullet}$) can be produced via the decomposition of ozone molecules in basic media, which have high oxidation potential, compared to the electrophilic O_3 molecules [12]. However, the simple ozonation process (SOP) has some disadvantages, such as the low solubility and stability of O_3 in water, which can reduce the elimination and mineralization rates of pollutants [13].

To overcome this issue, in the last decade, many researchers have reported different types of both heterogeneous and homogeneous catalysts for improving the ozonation efficiency, increasing the ozone decomposition, and generation more reactive oxygen species (ROS) [3,9,14]. Owing to the easy separation and rapid reusability of heterogeneous catalysts, these materials were widely used as promising candidates for the so-called Catalytic Ozonation Process (COP) [15,16]. Besides, other enhancements, such as the peroxone process (H_2O_2/O_3)

* Corresponding author.
E-mail address: moussavi@modares.ac.ir (G. Moussavi).

https://doi.org/10.1016/j.apcatb.2021.120786
Received 13 June 2021; Received in revised form 22 September 2021; Accepted 5 October 2021
Available online 6 October 2021

has received much attention in water treatment due to its capability to synergically produce $HO^{\bullet}$ [17,18]. The reaction rate constant of H_2O_2 with O_3 is strongly dependent on the reaction solution pH [19]. This value was reported to be 9.6×10^6 M^{-1} s^{-1}, and less than 0.1 M^{-1} s^{-1} when the pH value is 11.8, and 3.0, respectively [20]. This big difference between rate constant values is related to the formation of hydroperoxide ion (HO_2^-) at alkaline conditions that can continue the chain reactions of radical generation (Eqs. 1 and 2). Due to the high pK_a value of H_2O_2 (11.8), the efficiency of peroxone reaction is decreased by decreasing the pH value [21].

$$H_2O_2 \quad \leftrightarrow \quad H^+ + \quad HO_2^- \tag{1}$$

$$O_3 + \quad HO_2^- \quad \rightarrow \quad HO^{\bullet} + \quad O_2 + \quad O_2^{\bullet -} \tag{2}$$

In order to reduce the economic costs of COP and peroxone process, various heterogeneous catalysts, including metal oxides, such as MgO [3], SnO_2 [9], Fe_3O_4/MnO_2 [22], carbon-based materials, and metals or metal oxides on supports [16,23,24] have been widely used. Transition metal oxides containing various oxidation states are considered suitable catalysts for decomposition of ozone [25]. Moreover, the functional groups on the surface of metal oxides, as well as their chemical structure play a critical role in the formation of ROS and the improvement of the overall reaction efficiency [26]. In heterogeneous catalytic ozonation, especially in the presence of metal oxides, both Lewis and Bronsted acids sites work as catalytic centers [27]. For example, Zhang et al., used a ternary Mn-Fe-Ce/Al_2O_3 catalyst for the ozonation of phenol [28]. Due to presence of hydroxyl groups in the side of Bronsted acid site, and transition metal cations (Mn^{2+}, Fe^{3+}, and Ce^{3+}) in the side of Lewis acid site, high efficiency of phenol degradation was observed in Mn-Fe--Ce/Al_2O_3/O_3 system [28]. Hence, in catalytic ozonation processes, besides the direct oxidation by the ozone molecules, the active sites of the catalysts play vital role in decomposition of ozone and formation of reactive species [29]. Iron oxides, has been widely used in COP, due to their high surface area, and high catalytic activity [30]. Hematite (α-Fe_2O_3) is a stable structure of iron oxide that has been widely used as a non-toxic material in various applications, such as catalysis, photo-oxidation, photocatalysis, lithium-ion batteries and water-splitting [31,32], due to its excellent properties: high electrical conductivity, chemical stability, high activity, and high surface area with low particle size [33]. Different synthesis methods such as hydrothermal, micro-emulsion, sol-gel, and solvent evaporation have been reported for the fabrication of hematite, which can tune α-Fe_2O_3 towards different properties [34,35]. Nevertheless, the preparation of catalysts by a chemical route can increase the environmental concerns due to secondary pollution. Therefore, using natural materials with similarly convenient properties have been employed in environmental applications [36].

Owing to their low cost, easy use, non-toxicity, and environmentally friendly properties, the application of natural iron oxides has increased in catalytic reactions [37]. Fe-based mineral compounds such as pyrite, martite, chalcopyrite, magnetite, and hematite were used as promising candidates in AOPs [38]. The natural iron oxides are abundant in the nature, which impulse their use in environmental applications [39]. For instance, natural iron oxide minerals were developed and used as efficient catalysts for the removal and adsorption of arsenic [40]. Elfiad et al., reported high activity of natural α-Fe_2O_3 in reduction of 4-nitrophenol (4-NP) [31]. Based on their report, the calcination of natural iron at 450 °C could enhance the catalytic activity of natural iron oxide in reduction of 4-NP [31]. In a previous study, we investigated the activity of Hormuz Red Soil (HRS) collected from Hormuz Island in the south of Iran as a naturally occurring red soil source, in the activation of peroxymonosulfate, for the degradation of organic pollutant (diclofenac), and inactivation of bacteria [41].

Under this scope, in this study we used the calcinated HRS (C-HRS) as precursor of catalyst in O_3, and peroxone (O_3 +H_2O_2) processes. The singular properties of this soil (high hematite content, catalytic activity, size, stability and dispersibility) are used in a catalytic ozonation process, for the degradation of ACT from water; to the best of the authors' knowledge, it is the first time the catalytic activity of HRS in ozonation process for the removal of organic pollutants from water is reported. The various experimental conditions including catalyst dosage, ozone and H_2O_2 concentrations (peroxone system), and initial solution pH were investigated within the catalytic ozonation reaction, and the catalytic activity was determined. Moreover, the reaction mechanism was studied in detail, by using radical trapping experiments and the proposed mechanism of ACT degradation was reported.

2. Materials and methods

2.1. Chemicals and reagents

Hormuz red soil (HRS) as a naturally hematite-containing material was sampled from Hormuz Island in Iran, and used as a catalyst in this study as is, or after calcination at 600 °C under air atmosphere and named as C-HRS. Acetaminophen (ACT) powder was obtained from a local supplier (Aria Co. Iran). The stock solution was prepared by dissolving of 0.65 g of ACT in 1.0 L of deionized (DI) water, and stored at 4.0 ± 1.0 °C. Acetonitrile, sulfuric acid, methanol (MeOH), *tert*-butyl alcohol (TBA), ethanol, and *p*-benzoquinone (BQ) were purchased from Merck Company. Also, sodium hydroxide (NaOH), potassium iodide (KI), sodium bicarbonate ($NaHCO_3$), sodium sulfate (Na_2SO_4), sodium phosphate (Na_3PO_4), salicylic acid ($C_7H_6O_3$, SA), hydrogen peroxide solution (H_2O_2, 30% w/w), and titanium (VI) oxysulfate ($TiOSO_4$) were supplied from Sigma-Aldrich.

2.2. Analytical techniques: HRS and C-HRS characterization and reaction evolution

X-ray diffraction (XRD) patterns of samples were obtained by Philips X′Pert-MPD X-ray diffractometer with a Cu Kα radiation (λ = 1.54060 A°) in the 2Θ range of 10–80°. The functional groups of samples were identified by the Fourier transform infrared spectra (FT-IR, AB BOMER MB spectrophotometer) in the wavelength range from 500 to 4000 cm^{-1}. The structural composition was evaluated by using X-ray fluorescence (XRF) technique on a Philips-X′PERT-PW 2404 instrument. The morphology of samples was characterized by field emission scanning electron microscopy (FE-SEM, Mira3 Tascan), energy dispersive X-ray spectroscopy (EDX), and transmission electron microscopy (TEM, Philips-CM30 instrument). In order to investigate the oxidation state of the elements in the sample, X-ray photoelectron spectroscopy (XPS) was carried out on SPECS Phoibos 100 MCD5 hemispherical electron analyzed operating at a constant pass energy. Kα Mg (1253.6 eV) was the X-ray source employed together with a flood electron gun to compensate charge effects on the catalysts. Survey and high-resolution spectra were performed with an energy pass of 90 eV and step energy of 1.0 eV, and with an energy pass of 30 eV and step energy of 0.1 eV, respectively. The specific surface area and pore size distribution of samples were studied by using nitrogen (N_2) adsorption/desorption isotherms at 77 K (Micromeritics/Gemini-2372 analyzer).

In order to monitor the reaction solution, high pressure liquid chromatography (HPLC, Eclipse plus C18 column; 3.5 μm, Agilent Co) equipped with a UV detector at 242 nm was applied. The mobile phase was a mixture of phosphate buffer (pH=4.0), and acetonitrile with a volumetric ratio of 85:15, and injected with flow rate of 1.0 mL/min. The pH of reaction solution was measured by a Jenway pH-meter (Jenway Co. UK). The concentration of iron leaching during the reaction was measured by using inductively coupled plasma-atomic emission spectroscopy (ICP-AES) on Varian 730-ES spectrophotometer. Total organic carbon (TOC) of samples was measured by using a Shimadzu TOC Analyzer (TOC-L CSH/CSN). To obtain more information about intermediates products that were produced during ACT degradation, liquid chromatography-mass spectroscopy (LC-MS, 2010 A/Shimadzu)

coupled with an Eclipse Atlantis T3, C18 column (2.1 ×100 mm, 3.0 μ particle size) was applied at room temperature. The mobile phase of this analysis consisted of acetonitrile (containing 0.1% formic acid), and water (containing 0.1% formic acid), with injected flow rate 0.2 mL/min, and sample volume of 10.0 μL. Also, the following conditions were selected for the Mass spectrophotometer: gas nebulizer: nitrogen (N_2), capillary volt: 4.0 kV, Cone volt: 30 V, flow gas: 3.3 L/min, while source and desolation temperatures were 120 °C and 350 °C, respectively. UV-Vis spectrophotometer (Unico-UV 2100) was used for the evaluation of H_2O_2 concentration during the reaction via the addition of $TiOSO_4$ solution [42]. The pH_{zpc} value of catalyst was determined by using KNO_3 solution as electrolyte according to a previously published method [43].

2.3. Catalytic ozonation of Acetaminophen: experimental details

To investigate the catalytic activity of HRS and C-HRS, the catalytic ozonation process (COP) was conducted in a 150 mL glass-reactor with a sintered-glass diffuser installed at 1.0 cm distance from the bottom to diffuse the ozone gas into the reaction solution. The ozone was generated by an ozone generator (ARDA Co). The dose of ozone was constant, set at 1.2 mg O_3/min. The schematic of the reaction set-up is illustrated in Fig. 1. In a typical reaction, 50 mg of catalyst was dispersed in 50 mL of ACT solution (50 mg L^{-1}), the suspension was poured into the glass reactor, and the ozonation reaction was started at the dosage of 1.2 mg O_3/min. The reaction mixture was magnetically stirred at 100 rpm. After different interval reaction times, 1.0 mL of reaction solution was taken, and filtered by 0.22 μL PTFE membranes. Then the concentration of ACT was measured by using HPLC. In addition, KI solution was used to discharge the exhaust gas that produced by the reaction. A similar route was applied for the peroxone, and catalytic peroxone reactions while different concentrations of H_2O_2 solution was used during the processes.

Radical trapping experiments were applied to investigate the role of different reactive species during the reaction. Accordingly, various scavengers and inorganic ions including TBA, MeOH, BQ, SA, phosphate, sulfate, chloride, and carbonate ions were used in the reaction, while the rest of the reaction conditions ([ACT] = 50 mg L^{-1}, [catalyst] = 1.0 g L^{-1}, and Ozone dosage = 1.2 mg O_3/min) were kept constant. The concentration of TBA, and MeOH were 4.0 g L^{-1}, and the concentration of the other scavenger/inhibitors were selected to be 0.1 g L^{-1}. To study the residual concentration of H_2O_2 at the end of reaction, the reaction mixture was bubbled with N_2 gas to remove the ozone gas from the mixture. 1.0 mL of reaction solution was sampled and filtered by 0.22 μL PTFE membranes, and transferred into the cuvette and 20 μL of $TiOSO_4$ solution was added and mixed; the absorption was measured at 410 nm.

To investigate the reusability of C-HRS in catalytic ozonation of ACT, the catalyst was collected by centrifugation (5000 rpm for 10 min) at the end of the reaction. Then, the collected catalyst was washed three times with water/ethanol mixture to remove impurities and finally dried at 70 °C overnight. Afterward, the catalyst was re-used in COP under optimum reaction conditions ([catalyst] = 1.0 g L^{-1}, Ozone dosage = 1.2 mg O_3/min, pH = 7.0, and reaction time=10 min).

2.4. Kinetic analysis

The concentration of ACT was measured by using the following equation (Eq. 3), in which ACT_0, and ACT_t are the concentration of ACT at time zero, and t, respectively.

$$ACT \quad degradation \quad (\%) = \frac{ACT_0 - ACT_t}{ACT_0} \times 100 \tag{3}$$

In addition, the ACT mineralization was investigated by TOC measurement (Eq. 4).

$$Mineralization \quad (\%) = \frac{TOC_0 - TOC_t}{TOC_0} \times 100 \tag{4}$$

Where, TOC_0, and TOC_t are the ACT concentration at time 0, and t, respectively. Also, the kinetics of the reaction was evaluated by the pseudo-first order reaction model (Eq. 5) [43]:

$$\ln\left(\frac{C_t}{C_0}\right) = -k_{app}t \tag{5}$$

In which, C_0, C_t, and k_{app} are the ACT concentration at time 0, t, and rate constant value, respectively. The k_{app} value was calculated from the slope of ln (C_t/C_0) versus reaction time. Finally, the synergy (S) with involved processes was calculated by using following equation (Eq. 6) [44], where the k_{CO}, k_C, and k_O are the reaction rate of catalytic ozonation, catalyst alone (adsorption), and ozone, respectively. Values S > 1 show a synergy effect between involved processes, while S < 1 indicates an antagonistic effect [41].

$$S = \frac{k_{CO}}{k_C + k_O} \tag{6}$$

Also, the catalytic activity of processes was evaluated using following equation (Eq. 7) [3]:

$$\text{Catalytic activity} = [\text{ACT removal in COP} - (\text{ACT removal in SOP} + \text{ACT adsorption on C-HRS})] \tag{7}$$

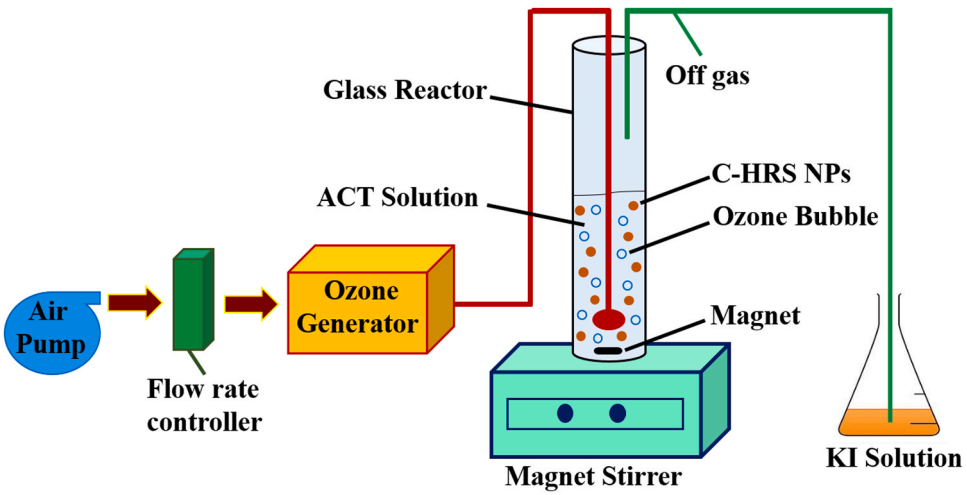

Fig. 1. Experimental set-up of the ozonation process used in this study.

3. Results and discussion

3.1. Characterization of the HRS and C-HRS catalysts

Fig. 2a shows the FT-IR spectra of HRS, and calcinated HRS (C-HRS). As it can be seen from the results, the absorption peaks centered at 478 cm^{-1}, and 552 cm^{-1} are assigned to the bending and stretching modes of the Fe-O bond in the rhombohedral lattice of hematite [45]. In addition, the absorption band located at 3425 cm^{-1} and 1630 cm^{-1} are related to the stretching and bending vibrations of hydroxyl groups, and/or water molecules, respectively [44]. The bending vibration modes at 792 cm^{-1}, and 1121 cm^{-1} are assigned to the stretching vibration of Fe-OH bond that indicated the presence of hydroxyl on the surface of catalyst [38]. These functional groups played critical role in formation of reactive species for the degradation of ACT in the presence of ozone molecules [26]. Also, the observed peak at 1065 cm^{-1} in FT-IR spectra of HRS, and C-HRS is attributed to the asymmetric stretching modes of Si-O-Si [46], which indicated the presence of SiO_2 in both samples.

The X-ray diffraction (XRD) patterns of samples were reported in Fig. 2b. In the XRD pattern of HRS, the diffraction peaks centered at 14.6°, 24.2°, 25.6°, 33.7°, 41.6°, 48.1°, 52.6°, 54.1°, 58.2°, 63.0°, 65.6°, and 76.0° are attributed to the (012), (104), (110), (202), (024), (018), (214), (300), (208), (119), (220), and (220) crystalline planes of hematite structure (JCPDS No. 33-0664) [47]. Moreover, the diffraction peaks related to goethite (α-FeOOH) were observed in XRD pattern of HRS (JCPDS No. 08-097) [31]. After calcination of HRS at 600 °C, these peaks disappeared, and all observed (remaining) peaks are related to α-Fe_2O_3 structure. In fact, during the calcination, the goethite structure was dehydroxylated and converted to hematite structure [48]. The additional peaks centered at 21.8°, and 42.7° are assigned to the SiO_2 structure in the samples which were matched with the JCPDS No. 58-0796 [41]. XRD patterns confirmed the presence of α-Fe_2O_3 and SiO_2 in C-HRS catalyst.

The chemical composition of samples was investigated by XRF. The summary of the obtained results is reported in Table 1. Based on the results, the HRS contained a high amount of α-Fe_2O_3 (56.95%), and SiO_2 (17.89%). Other oxides including SO_3, CaO, Al_2O_3, MgO, and MnO were found in HRS with different weight %. The total weight percent of HRS, and C-HRS was composed of α-Fe_2O_3, and SiO_2 with the Fe/Si ratio of 3.18, and 3.09, respectively. The red color of HRS, as well as C-HRS, is related to the high %wt. of iron. So, hematite and silicon dioxide mainly compose the HRS, and C-HRS catalysts. The low values of Loss on Ignition (LOI) for both samples indicates the organic content of samples is low. This parameter was obtained to be 7.76%, and 5.50% for HRS, and C-HRS, respectively, which can be related to carbon dioxide evaporation [31]. As such, the XRF analysis confirmed the above explained XRD results.

Fig. 3 shows the FE-SEM images of HRS (Fig. 3a), and C-HRS (Fig. 3b-d) nanoparticles (NPs). Based on the results, the particles have an irregular polyhedron structure. This structure was confirmed via TEM images (Fig. 3e-h). Figs. 3i and 3j show the particle size distribution of HRS, C-HRS NPs, respectively. This value was calculated to be 211 nm, and 142.5 nm for the HRS, and C-HRS, respectively. Compared to HRS NPs, the average crystalline size of catalyst was decreased during the annealing treatment. Similar behavior was reported for the natural hematite [31]. The SEM-mapping confirmed the presence of iron (Fe), silicon (Si), and oxygen (O) as main elements in C-HRS NPs (Fig. 3k-m). Moreover, the elemental composition of C-HRS was investigated by EDX analysis (Fig. 3n). According to the EDX spectrum, the presence of iron (Fe), silicon (Si), and oxygen (O) was confirmed.

In order to determine the oxidation states of the elements in HRS and C-HRS NPs, XPS analysis was applied. According to the obtained results, Fe, O, C, and Si were observed in both HRS and C-HRS (Fig. 4a, and f). As it can be seen from the Fe 2p spectrum (Fig. 4b, and g), the deconvolution of Fe $2p_{3/2}$ included three peaks, observed at 708.8 eV, 711.6 eV and 714.3 eV in the case of HRS, while in C-HRS a shift towards lower binding energies was observed, the values being 708.5 eV, 711.5 eV, and 713.8 eV. Also, the peaks centered at 722.5 and 724.9 eV are assigned to the Fe $2p_{1/2}$ for HRS, and at lower values of binding energies for C-HRS (722.1 eV, and 724.7 eV). These peaks are related to the existence of Fe^{3+} species in both samples [49]. The shift in the binding energies between HRS and C-HRS NPs can be explained due to the presence of α-FeOOH in HRS, which exhibit higher values than those of α-Fe_2O_3 [50]. Hence, the presence of α-Fe_2O_3 was validated anew in C-HRS. The XPS spectrum of O 1 s of HRS (Fig. 4c) shows two main peaks at 530.1 eV and 527.9 eV that are assigned to the Fe-O and O-H and/or H-OH [44,51]. In the case of C-HRS an additional peak at 529.2 eV was also determined, which is attributed to the oxygen vacancies formed during the calcination process that can improve the catalytic activity. Several authors have reported the vital role of the oxygen vacancies in the notable catalytic performance of different heterogeneous catalysts [52–54]. Based on the Si 2p spectrum (Fig. 4d, and i), the binding energy located at 100.9 eV is related to the Si-O bond in both HRS and C-HRS [51]. So, the presence of α-Fe_2O_3, and SiO_2 in C-HRS was confirmed by the XPS results. Due to natural origin of the catalyst, the spectra of C 1 s was also investigated. As it can be seen from the corresponding spectrum of HRS (Fig. 4e), the binding energies located at 282.2, 283.1 and 283.9 correspond to the Si-C, C-O and C-S-C, respectively [51]. Besides, two additional peaks at 283.9 eV and 286.6 eV, which are attributed to C-C and C-OH, respectively, were also observed in C-HRS catalyst. The characteristic peak of C-S-C bond in HRS and C-HRS NPs can be explained due to the presence of organic matter with Sulfur in its composition, such as fulvic and humic acids [55]. It should be noted that HRS originates from soil, which typically contains around 5.0% of organic matter [56]. In overall, the XPS results

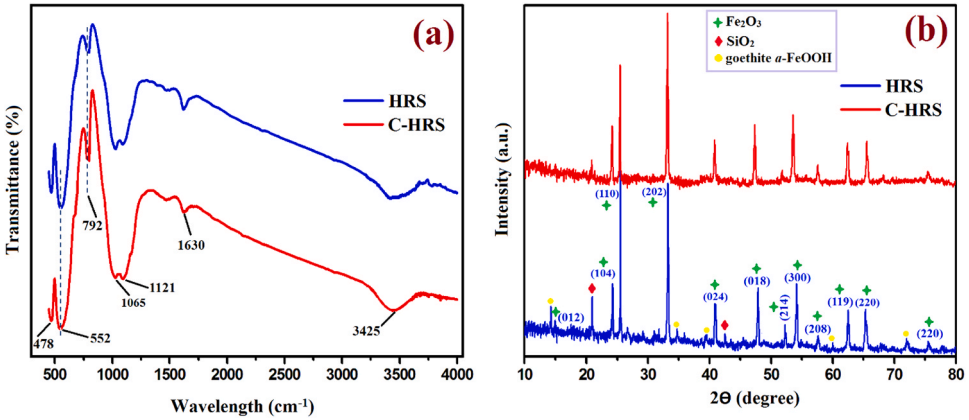

Fig. 2. FT-IR (a), and XRD (b) spectra of HRS and C-HRS nanoparticles.

Table 1
Chemical composition, and ignition loss (LOI) of HRS, and C-HRS.

Compounds	α-Fe_2O_3	SiO_2	SO_3	CaO	Al_2O_3	MgO	K_2O	Na_2O	Cl	MnO	LOI	Others
HRS	56.95	17.89	5.60	3.81	3.80	1.61	0.84	0.80	0.41	0.22	7.76	0.31
C-HRS	57.95	18.72	5.84	3.78	3.82	1.84	0.80	0.84	0.37	0.20	5.50	0.34

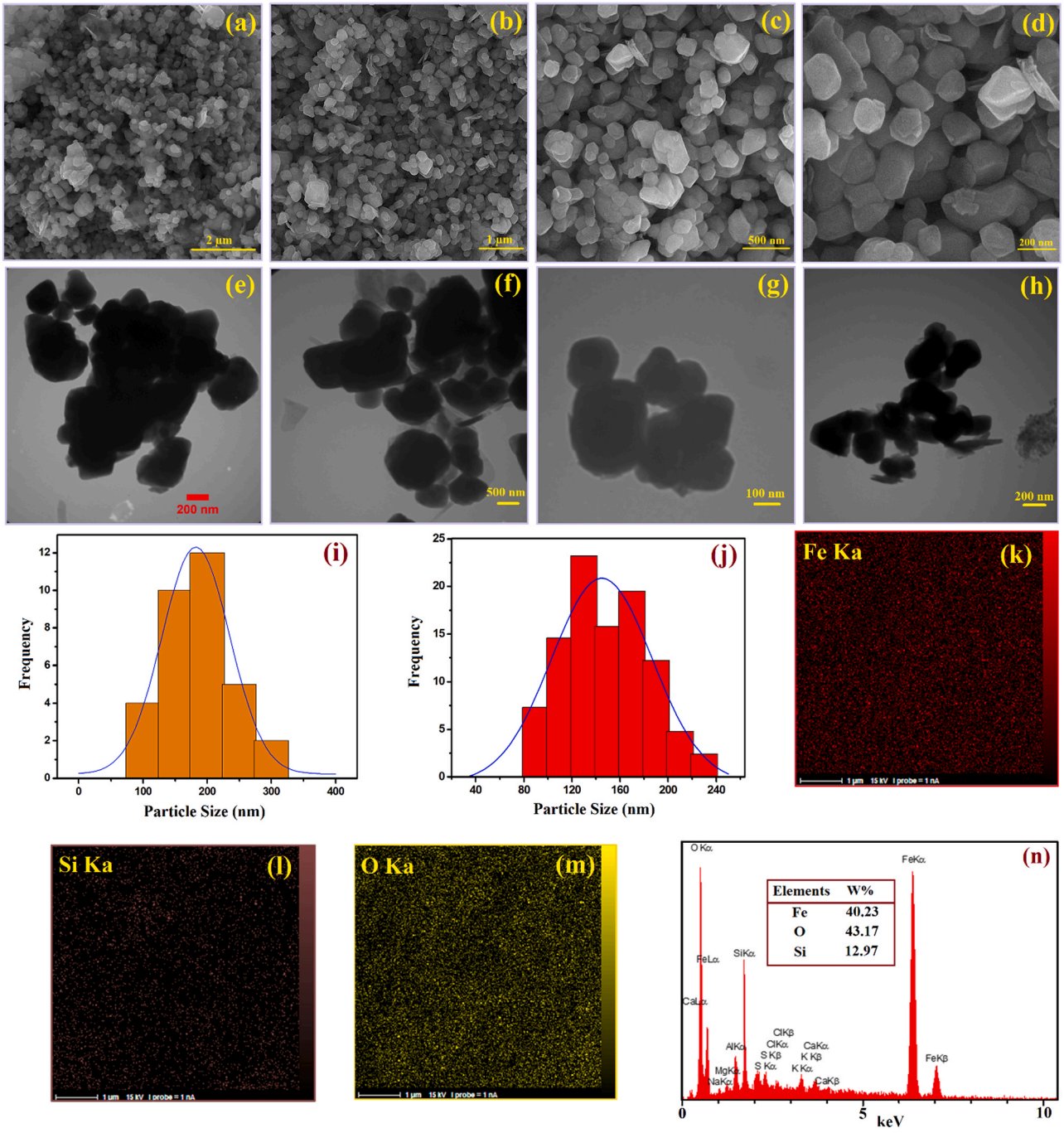

Fig. 3. FE-SEM images of HRS (a), and C-HRS (b-d). TEM images of HRS (e and f), and C-HRS (g and h). The particle size distribution histogram of HRS (i), and C-HRS (j) NPs. Elemental mapping of Fe (k), Si (l), and O (m), and EDX spectrum (n) of C-HRS NPs.

confirmed the existence of α-Fe_2O_3 in C-HRS NPs. Moreover, the presence of hydroxyl groups and oxygen vacancies on the surface of the catalyst, which are expected to play a vital role in the formation of reactive species, was also confirmed from the XPS analysis.

Fig. 5 illustrates the N_2 adsorption/desorption isotherms of HRS, and C-HRS NPs. Based on these results, after the calcination process the BET surface area of HRS NPs was decreased and changed from 5.17 $m^2\,g^{-1}$ to 3.63 $m^2\ g^{-1}$. The calcination method can affect the overall powder properties, and the reduction of its surface area is within the expected modifications [57]. Also, both samples showed the type IV isotherm

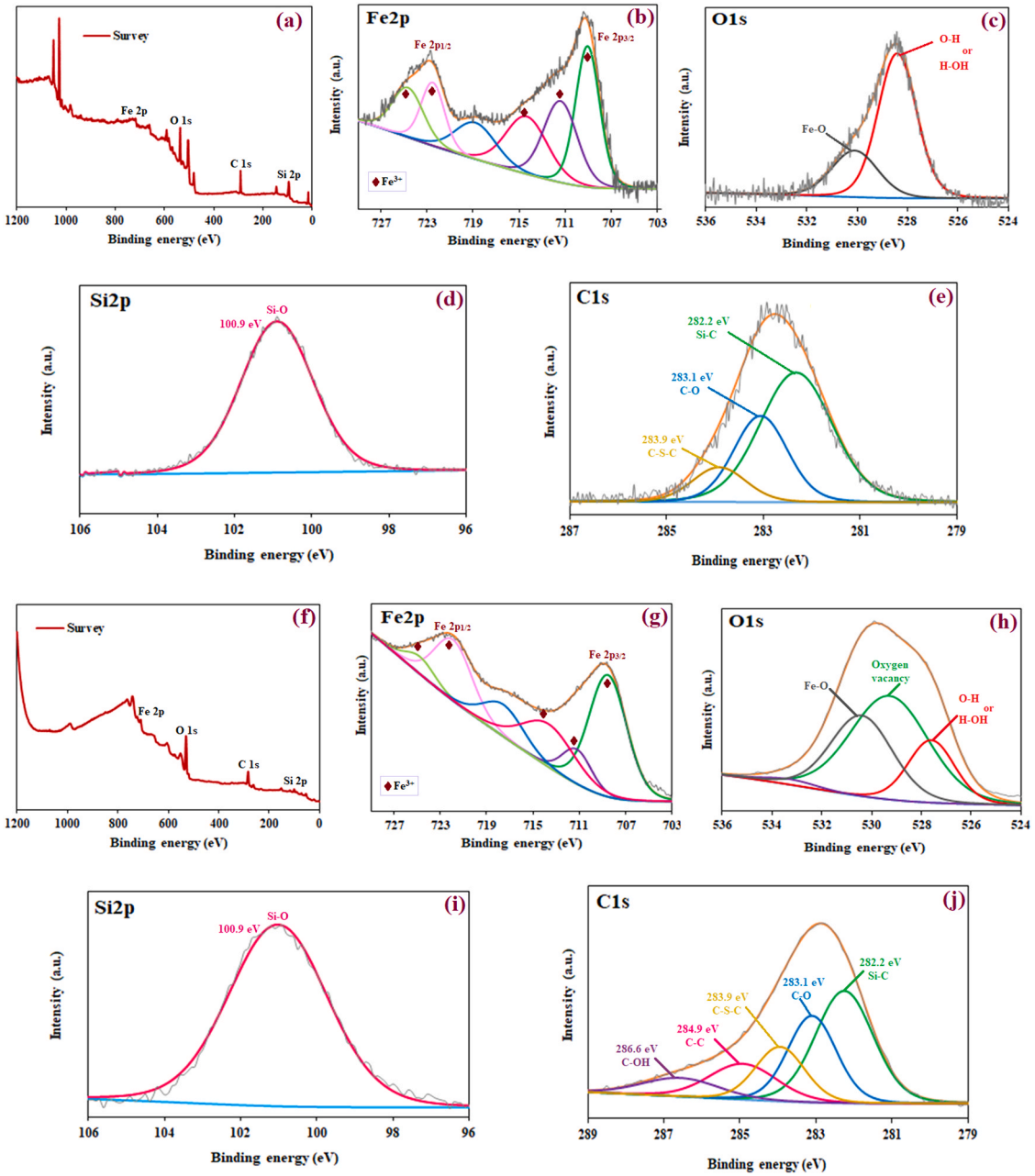

Fig. 4. XPS survey spectra of HRS (a), and the high-resolution spectra of Fe 2p (b), O 1 s (c), Si 2p (d), and C 1 s (e). Survey spectra of C-HRS (f), and the high-resolution spectra of Fe 2p (g), O 1 s (h), Si 2p (i), and C 1 s (j).

with H3-type hysteresis loop, which confirmed their mesoporous structure [44]. In addition, the pore size distribution curves of the samples indicate the presence of a mesoporous structure (4.0–50 nm) for the both samples (See the insert curves of Fig. 5). This value was obtained to be 9.23 nm, and 12.56 nm for the HRS, and C-HRS, respectively, which is in accordance to the relevant literature [31,58], where the pore diameter of catalysts was increased during calcination.

3.2. The activity of natural hematite towards the catalytic ozonation of Acetaminophen

3.2.1. Catalytic activity of the samples and effect of catalyst dosage

The catalytic activity of the natural minerals was evaluated in catalytic ozonation process (COP) of ACT. As it can be seen from the results, ACT and catalyst mixing (see Materials and Methods) leads to saturation and adsorption is minimal; the small increase in C-HRS is a result of the higher pore diameter. Simple ozonation (SOP) has a moderate effect in ACT degradation, with a 30% elimination attained within the first 10 min of the reaction. However, the addition of HRS and the conversion to a COP significantly enhances ACT removal (90% in 10 min). As such, it is safe to propose that the presence of HRS induces the generation of reactive species that assist in the ACT degradation.

The catalytic ozonation efficiency of ACT was enhanced in the presence of C-HRS compared to HRS (Fig. 6a), with 80% removal in the first 4 min of the reaction, followed by a reactant-limited step. In heterogeneous systems, the smaller particle size show higher catalytic activity, which is related to the greater surface area per unit mass of catalyst [59,60]. The k_{app} value for the SOP, and COPs in the presence of HRS, and C-HRS were calculated form the slope of ln (C_t/C_0)-time (Fig. 6b). The k_{app} value for C-HRS/O_3 process (0.35 min^{-1}) was 1.84 times higher than HRS/O_3 system (0.1901 min^{-1}), meanwhile these values were obtained to be 0.032 min^{-1}, and 0.0063 min^{-1} for SOP, and

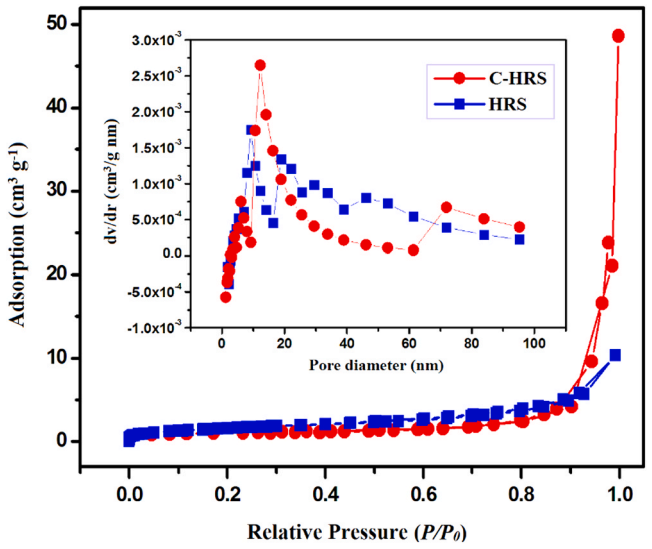

Fig. 5. N_2 adsorption/desorption isotherms of HRS, and C-HRS NPs.

catalytic adsorption process, respectively. The synergy factors were calculated to be 9.1, and 5.0 for catalytic ozonation by using C-HRS and HRS NPs, respectively, which indicated the high complementarity of the processes involved in the catalytic ozonation.

Following, the effect of catalyst concentration was evaluated in COP (C-HRS/O_3) of ACT. Therefore, the reaction was carried out under various catalyst concentrations in the range between 0.2 and 1.4 g L^{-1} (Fig. 7a). Compared to SOP, by the addition of catalyst (0.2 g L^{-1}) into the reaction, its efficiency was increased from 29% to 62.3%. This result indicated the important role of the catalyst in the formation of reactive species. By increasing the catalyst dosage up to the 1.0 g L^{-1}, the removal efficiency of ACT was increased, and the highest value was obtained at 1.0 g L^{-1} (complete oxidation of ACT during 10 min). Meanwhile, under higher dosage (1.4 g L^{-1}), the reaction efficiency remained constant, which indicated that sufficient active sites are available for the ozone decomposition, and degradation of 50 mg L^{-1} of ACT solution.

To better understand the catalytic activity, the k_{app} values of the various reactions were calculated by Eq. 5, and the results are reported in Fig. 7b. Compared to the SOP, the k_{app} value for the COP, when the concentration of catalyst was 1.0 g L^{-1}, was 10.9 times higher than SOP (0.032 min^{-1}). In fact, at high concentration of catalyst, more active sites are available for the ozone-catalyst interaction that can increase the formation of reactive species [61]. Fig. 7c demonstrates the catalytic activity of reaction by the various concentrations of catalyst. According to the results, by increasing the catalyst doses from 0.2 to 1.0 g L^{-1}, catalytic activity was increased, while at higher concentrations (more than 1.0 g L^{-1}) the catalytic activity was constant. So, 1.0 g L^{-1} (50 mg of C-HRS) was selected as the optimum catalyst value in this reaction.

3.2.2. *Effect of ozone concentration*

To investigate the effect of ozone dosage on ACT degradation, the reaction was carried out under different concentrations of ozone (0.6–1.8 mg O_3 min^{-1}) while the other conditions ([ACT] = 50 mg L^{-1}, and [catalyst] = 1.0 g L^{-1}) were kept constant, and the results are shown in Fig. 7d. By increasing the O_3 concentration from 0.6 mg min^{-1} to 1.2 mg min^{-1}, the reaction efficiency was increased from 68% to 100% that highlighted the critical role of ozone concentration on ACT degradation. This behavior can be related to the abundance of ozone molecules that can enhance the possibility of interaction with ACT molecules. Similar behavior was observed in the *m*-MgO/O_3 system for oxidation of ACT [62]. In COP, the reaction efficiency increased linearly from 68% to 100% within 10 min when the ozone concentration was 0.6 mg O_3 min^{-1}, and 1.2 mg O_3 min^{-1}, respectively. In order to better understand the role of ozone dosage on ACT degradation, the catalytic activity was calculated for the different dosages, and the results are illustrated in Fig. 7d. As it can be seen from the results, the highest catalytic activity was obtained at 1.2 mg O_3/min, while by increasing the ozone dosage the catalytic activity was decreased, as previously proposed in antagonistic reactions [9]. So, this concentration (1.2 mg O_3/min) was selected as the optimum value for this reaction.

3.2.3. *Effect of initial solution pH on the catalytic ozonation of ACT*

In heterogeneous COP, the catalytic efficiency is strongly depended on the surface properties of catalyst, and hence, the solution pH can affect the speciation of the surface-active sites [63]. In order to study the effect of initial pH on removal efficiency of ACT, COP was carried out under different pH values ranging from 3.0 to 11. Fig. 8a shows the effect of initial pH on ACT removal efficiency. In COP, by increasing the pH value from 3.0 to 7.0, the %ACT removal was increased and complete removal was obtained at pH = 7.0, within 10 min of reaction. Although, at high pH values (pHs = 9.0, and 11), only 6.0, and 4.0 min was enough for the complete removal of ACT (50 mg L^{-1}), respectively. Kinetic-wise, the k_{app} values were calculated by using Eq. 5, and the results are illustrated in Fig. 8b. Based on the results, the k_{app} values of COP of ACT at pH= 11 (1.52 min^{-1}) was 6.1, 4.5, and 3.6 times higher than the calculated values at pHs = 3.0, 5.0, and 7.0, respectively. At basic media and neutral values, the COP was faster than acidic conditions. According to the results, the highest catalytic activity was obtained at pH= 7.0, while by the increasing pH values, the activity decreased, and the lowest amount (37.3%) was obtained at pH= 11. So, pH= 7.0 was selected as the optimum pH value for this reaction.

As reflected above, the pH is a parameter that affects the system in a

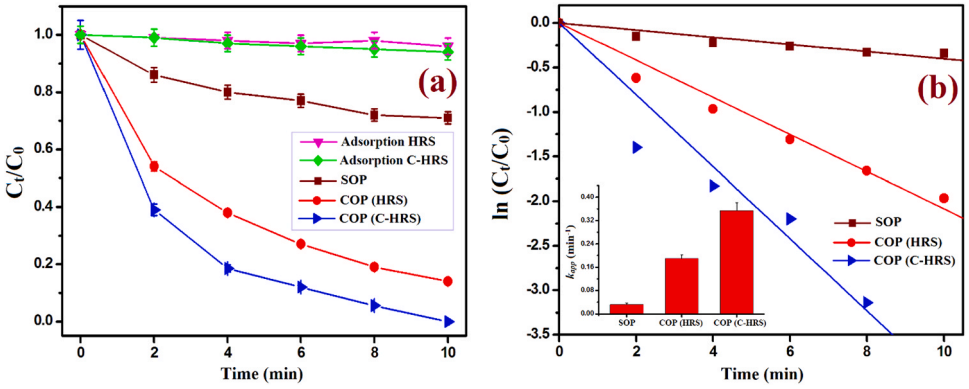

Fig. 6. (a) Plots of C_t/C_0, and (b) ln (C_t/C_0) versus reaction times for different processes (insert curve shows the k_{app} values of various reactions). Reaction conditions: [ACT] = 50 mg L^{-1}, [catalyst] = 1.0 g L^{-1}, Ozone dosage= 1.2 mg O_3/min, and pH= 7.0.

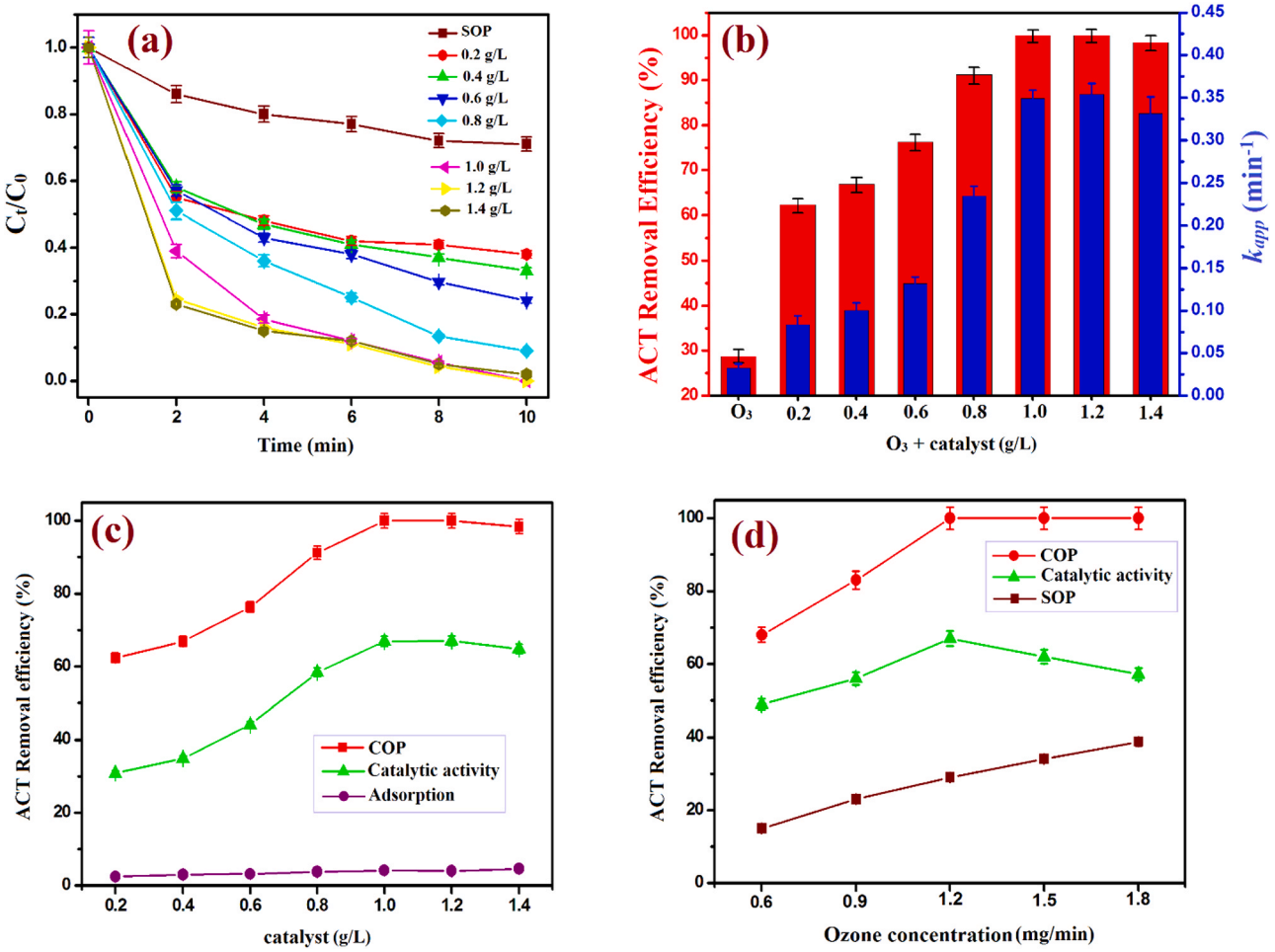

Fig. 7. (a) The plots of C_t/C_0 versus reaction time for COPs in the presence of different concentrations of C-HRS NPs, and (b) PFO constant values of various COPs. (c) Effect of various dosages of catalyst, and (d) ozone concentration on ACT degradation (Reaction conditions: [ACT] = 50 mg L^{-1}, [catalyst] = 1.0 g L^{-1}, and reaction time: 10 min).

multiple manner. As such, we studied the ACT adsorption, SOP, and COP through various values of initial pH solution. There is not any change on the adsorption of ACT on the surface of C-HRS under various pH values (Fig. 8c), which indicated the initial solution pH cannot affect ACT adsorption value on the surface of the catalyst. The degradation efficiency of ACT was increased in the SOP with increasing of pH values. By increasing the pH value from 7.0 to 11.0, the reaction efficiency was enhanced from 29% to 57%. This behavior can be related to the acceleration of ozone mass transfer, and ozone decomposition, at higher reaction solution pH [3,64], which can produce more hydroxyl radicals ($HO^{\bullet}$) for the degradation of ACT. $HO^{\bullet}$ is the main reactive species at high pH values, which has higher oxidative power compared to ozone molecules [63,65]. This behavior corresponds to the high concentration of hydroxide ions (HO^{-}) resulting greater formation of $HO^{\bullet}$ as main reactive species in this reaction.

Based on the pK_a value of ACT (pK_a=9.38), the ionic form of ACT ($C_8H_8NO_2^{-}$) is the dominant form at pH > pK_a, while the molecular form ($C_8H_9NO_2$) is the prevailing form at pH < pK_a [62,66]. So, at the optimum pH value, the ACT is in the form that can easily react with generated $HO^{\bullet}$ in the reaction media. In addition, the pH_{zpc} value of C-HRS was found to be 7.7, which indicated the surface of catalyst is positive at pH < pH_{zpc}, and is negative at pH > pH_{zpc}. Due to the negative charge of ACT and surface of catalyst at high pH value, the interaction between ACT and surface of catalyst was decreased which led to the decrease of the catalytic activity (Fig. 8c). Compared to SOP, the high removal efficiency that was obtained in COP can indicate the role of catalyst in ozone decomposition rate, as well as the formation of $HO^{\bullet}$.

As it is made clear from the above measurements, there are two different pathways for the ozone-mediated reactions, including direct and indirect pathways that depend on solution pH. At acidic media, the molecular ozone is the dominant oxidant, while at basic media (pH > 7.0) $HO^{\bullet}$ is the main oxidant [65]. In fact, the HO^{-} works as initiator of the production $HO^{\bullet}$ and increase the decomposition rate of O_3. So, due to the lack of HO^{-} concentration at acidic media, the lowest reaction efficiency was obtained at these values (pH = 3.0 and 5.0). On the other hand, the oxidation potential of $HO^{\bullet}$ ($E^0 = 2.80$ V) is higher than oxidation potential of O_3 molecules ($E^0 = 2.08$ V), which indicated that radical oxidation is faster than direct reaction [65]. Therefore, in alkaline conditions, radical reactions are responsible for ACT degradation. According to Eqs. (8–12), the reaction of ozone molecules with HO^{-}, and hydroperoxide ion (HO_2^{-}) work as initiation reactions of O_3 decomposition in water (Eqs. 8 and 9) [67]. In propagation reactions, the generated hydroperoxyl radical ($HO_2^{\bullet}$) can produce superoxide radical ($O_2^{\bullet-}$) (Eq. 10), which play a critical role in formation of ozonide ion radical ($O_3^{\bullet-}$) (Eq. 11). The $O_3^{\bullet-}$ can participate in generation of $HO^{\bullet}$ (Eq. 12). Therefore, the alkaline conditions were the most favorable for the ozonation process.

$$O_3 + HO^{-} \rightarrow HO_2^{-} + O_2 \quad k = 40 \quad M^{-1}s^{-1} \tag{8}$$

$$O_3 + HO_2^{-} \rightarrow HO_2^{\bullet} + O_3^{\bullet-} \quad k = 2.2 \times 10^6 \quad M^{-1}s^{-1} \tag{9}$$

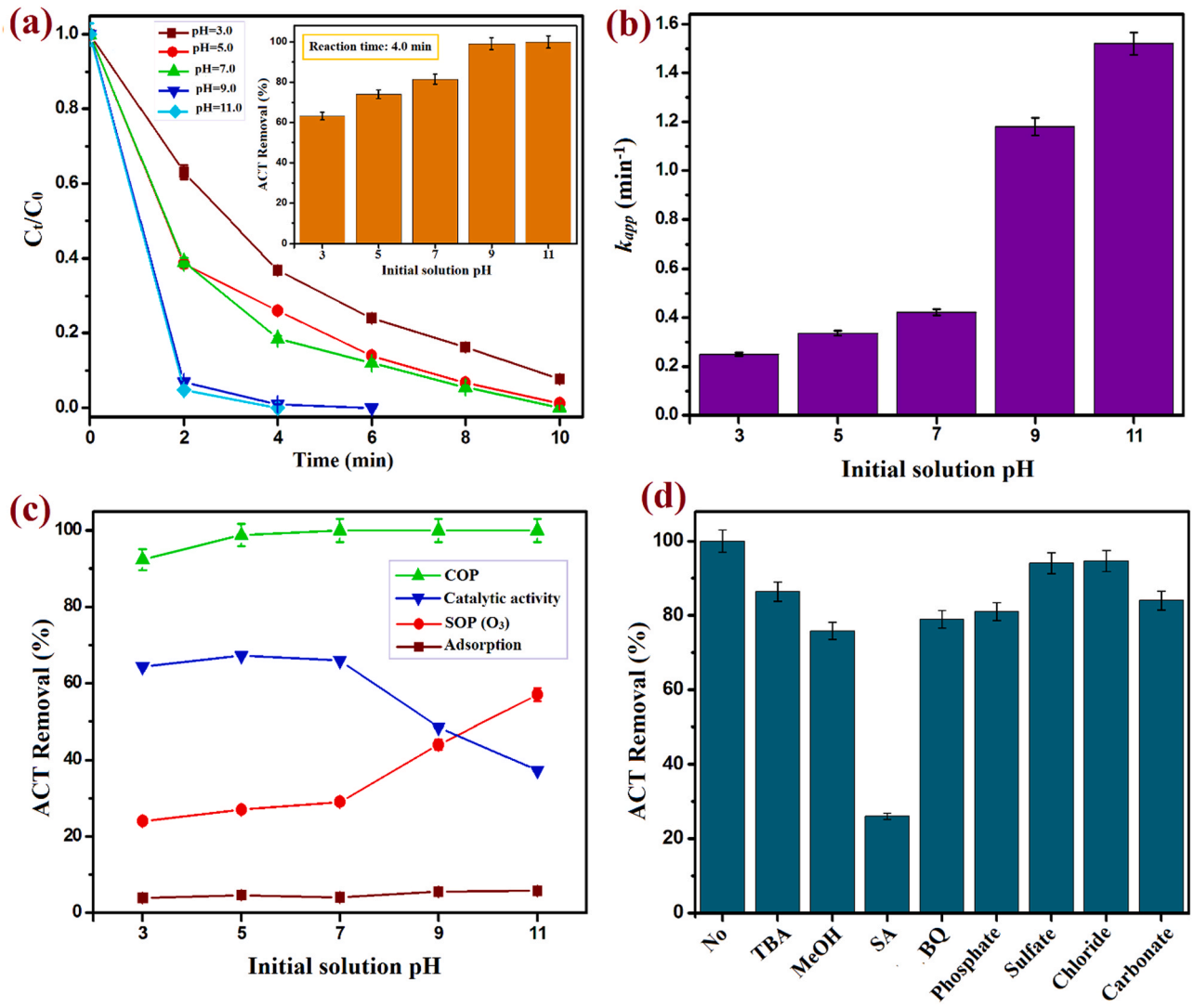

Fig. 8. (a) Plots of C_t/C_0 of ACT oxidation under various pH values, (b) k_{app} values of COP under different initial pH solution, and (c) effect of initial pH values on SOP, adsorption, and COP. (d) Effect of different scavengers/inhibitors on catalytic ozonation of ACT (Reaction condition: [ACT] = 50 mg L^{-1}, [catalyst] = 1.0 g L^{-1}, Ozone dosage=1.2 mg O_3/min, and pH=7.0).

$$HO_2^{\bullet} \rightarrow O_2^{\bullet -} + H^+ \quad k = 7.9 \times 10^5 \ s^{-1} \tag{10}$$

$$O_3 + O_2^{\bullet -} \rightarrow O_2 + O_3^{\bullet -} \quad k = 1.6 \times 10^9 \ M^{-1}s^{-1} \tag{11}$$

$$O_3^{\bullet -} + H_2O \rightarrow HO^{\bullet} + O_2 + HO^- \quad k = 20 - 30 \ M^{-1}s^{-1} \tag{12}$$

3.2.4. Catalytic peroxone process

In order to investigate the role of H_2O_2 in the enhancement of ozonation efficacy (i.e. peroxone process), different concentrations of H_2O_2 (10, 20, 30, and 40 mM) were used while the other (optimal) reaction conditions were kept constant; the results are reported in Fig. 9a, b. According to the results, by addition of hydrogen peroxide the reaction efficiency was improved, related to formation of a higher number of $HO^{\bullet}$ and faster decomposition of O_3 molecules compared to ozone alone. Our natural catalyst had vital role in the induction of the heterogeneous peroxone reaction. The presence of Fe^{3+} species in the catalyst (based on the XPS results) can participate in the generation of $HO_2^{\bullet}$ (Eq. 13) via the reaction with H_2O_2 (Fenton-like reaction). The Fe^{2+} species that are produced from the cyclic conversion of Fe^{3+} to Fe^{2+}, can also react with hydrogen peroxide and generate $HO^{\bullet}$ (Eqs. 14 and 15) [68]. The k_{app} value for Fenton (catalyst + H_2O_2) reaction was calculated to be 0.138 min^{-1}, while for H_2O_2 alone, no change in ACT concentration was observed during 10 min. This result confirmed the role of C-HRS catalyst in the formation of $HO^{\bullet}$ in the presence of H_2O_2 (Fenton reaction). According to the results, the catalytic peroxone process showed the highest activity in ACT degradation (Fig. 9a), and only 2 min were enough for the complete removal of this pollutant from the reaction media. This confirmed that the presence of H_2O_2 in COP can augment the generation of reactive species: the synergy between the catalyst, ozone, and H_2O_2, can accelerate the formation of $HO^{\bullet}$, resulting in the enhancement of the reaction kinetics.

$$Fe^{3+} + H_2O_2 \rightarrow Fe^{2+} + HO_2^{\bullet} + H^+ \tag{13}$$

$$Fe^{3+} + HO_2^{\bullet} \rightarrow Fe^{2+} + O_2 + H^+ \tag{14}$$

$$Fe^{2+} + H_2O_2 + H^+ \rightarrow Fe^{3+} + HO^{\bullet} + H_2O \tag{15}$$

In the developed C-HRS/O_3/H_2O_2 process, the highest efficiency and k_{app} value were observed in the presence of 20 mM of H_2O_2. However, at higher concentrations of H_2O_2 (30, and 40 mM), the reaction efficiency was decreased due to self-scavenging of hydroxyl radicals by the excess amount of H_2O_2, resulting in the formation of the less reactive hydroperoxyl radical ($HO_2^{\bullet}$) (Eq. 16) [69]. Compared to hydroxyl radical (E^0 = 2.80 V) and ozone molecules (E^0 = 2.08 V), the oxidation ability of

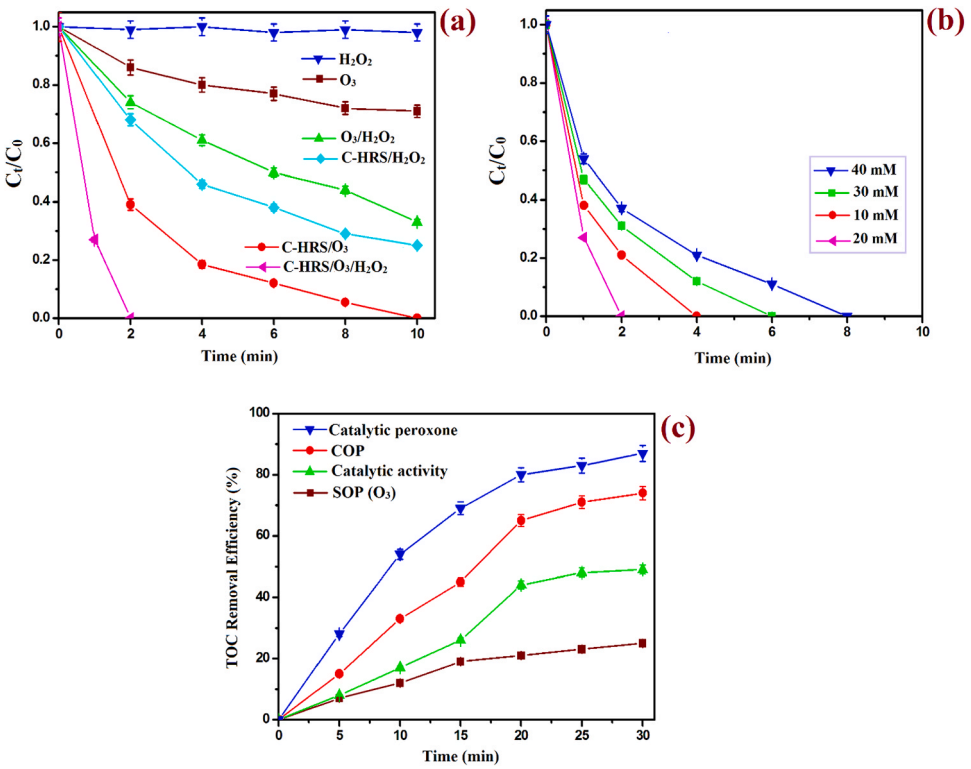

Fig. 9. ACT degradation through different reactions (a), and effect of various concentration of H_2O_2 on degradation of ACT through C-HRS/O_3/H_2O_2 process (b). TOC removal efficiency and catalytic activity of C-HRS NPs as function of reaction time (c).

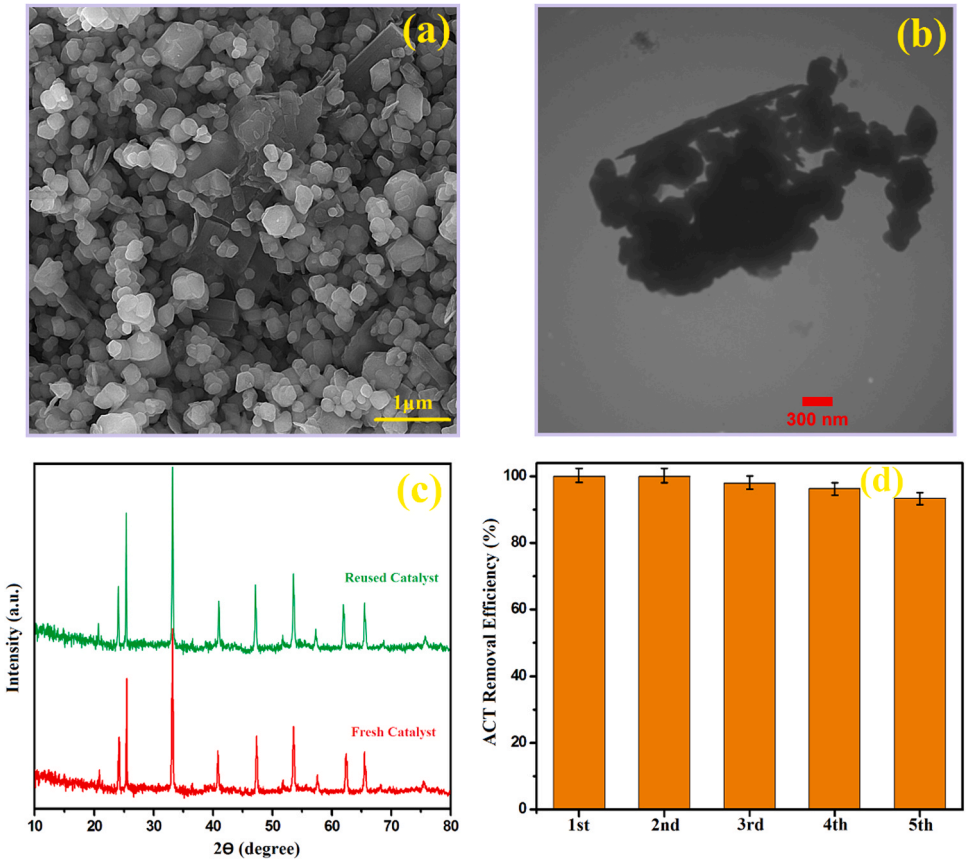

Fig. 10. SEM (a), and TEM (b) images of reused catalyst. XRD pattern of fresh and reused catalyst after 5th runs (c). ACT removal efficiency in various catalytic cycles (d).

$HO_2^{\bullet}$ is low ($E^0 = 1.44$ V) that can decrease the reaction efficiency [65,70,71]. So, 20 mM was used as the optimum value of H_2O_2 in catalytic peroxone reaction.

$$H_2O_2 + HO^{\bullet} \rightarrow HO_2^{\bullet} + H_2O \quad (16)$$

In order to evaluate the efficiency of the reaction, the concentration of consumed H_2O_2 in catalytic peroxone, and O_3/H_2O_2 processes was determined at the end of the reaction. The highest utilization of H_2O_2 was observed for the C-HRS/O_3/H_2O_2 system, leaving a low amount of residual H_2O_2 (0.8 mM), while in the O_3/H_2O_2 process this value was determined to be 9.7 mM. According to these results, the reaction between ozone and hydrogen peroxide was further promoted in the presence of the C-HRS catalyst.

Fig. 9c illustrates the TOC removal efficiency of ACT as a function of the reaction time. In SOP (O_3 alone), the TOC removal efficiency was increased by increasing the reaction time and the highest value was obtained within 30 min (25%). Compared to SOP, the TOC removal efficiency of ACT was dramatically increased in the presence of the C-HRS catalyst. The mineralization of ACT in COP was increased from 33% at the reaction time of 10 min to 74% at reaction time of 30 min. The highest TOC removal was obtained for catalytic peroxone reaction (87% TOC removal within 30 min), owing to presence of more reactive species that participated on ACT mineralization. Therefore, these results confirmed the high potential of C-HRS in degradation and mineralization of ACT in COP and peroxone processes.

3.3. Catalyst stability and reusability

The recyclability of catalyst is an important parameter for its wider application in a potential real-world application. So, the stability of the current morphology and crystalline structure of C-HRS were investigated by using SEM, TEM, and XRD analysis (Fig. 10a–c). No difference was observed in the SEM, and TEM images of reused catalyst compared to fresh catalyst that confirmed the high stability of C-HRS morphology during COP of ACT (Fig. 10a, b). According to the XRD pattern of reused catalyst (Fig. 10c), all characteristic peaks related to the α-Fe_2O_3 were found anew, which indicated the high crystal stability of catalyst after five catalytic runs. To evaluate the catalytic activity of reused catalyst in ozonation of ACT, the reused catalyst was tested in consecutive catalytic cycles under optimum reaction conditions ([ACT] = 50 mg L^{-1}, [catalyst] = 1.0 g L^{-1}, pH = 7.0, [O_3] = 1.2 mg min^{-1}, and Reaction time =10 min), and the obtained results are reported in Fig. 10d. Based on the results, C-HRS showed excellent catalytic performance after five catalytic cycles, and more than 93% of ACT was removed from reaction media within 10 min. To assess the structural (physicochemical) stability of catalyst and amount of metal leaching during the reaction, the concentration of iron was evaluated by ICP-AES analysis. This value was obtained to be 0.025 mg L^{-1}, and 0.012 mg L^{-1} when the HRS and C-HRS were used in the reaction, respectively. The standard value of Fe in EU, and China for drinking water was reported to be 0.2 mg L^{-1}, and 0.3 mg L^{-1}, respectively [72]. Hence, according to the ICP results, low amount of Fe was leached from catalyst to reaction solution, and high stability was observed for C-HRS NPs.

3.4. Proposed mechanism of ACT degradation in COP

As mentioned before, there are three main mechanisms that are involved in the catalytic ozonation of ACT: i) direct interaction of dissolved ozone molecules with ACT, ii) radical degradation of ACT with $HO^{\bullet}$ in bulk reactions, and iii) indirect reaction between generated radicals produced by the interaction between O_3 molecules and the catalyst. In order to evaluate the role of reactive species in COP degradation of ACT, various scavengers and inhibitors including TBA, MeOH, SA, BQ, carbonate, sulfate, phosphate, and chloride were employed. The obtained results are depicted in Fig. 8d. Among the different scavengers used for the trapping of $HO^{\bullet}$, the lowest efficiency was obtained in the presence of SA (only 26% removal within 10 min). This behavior is related to the reaction rate constant value of this scavenger with $HO^{\bullet}$ that reported to be 2.2×10^{10} M^{-1} s^{-1} [73], while this value was reported to be 9.0×10^8 M^{-1} s^{-1}, and $(3.6–7.8) \times 10^8$ M^{-1} s^{-1} for MeOH, and TBA, respectively [49]. In fact, the reaction of SA inhibitor with the $HO^{\bullet}$ was 3.1 times higher than the rate of ACT molecules with $HO^{\bullet}$ (7.1×10^9 M^{-1} s^{-1}) [72,74]. To investigate the role of superoxide radical ($O_2^{\bullet-}$) during the COP, BQ was employed. In the presence of BQ as $O_2^{\bullet-}$ scavenger, the reaction efficiency was decreased and reached 79% during 10 min (Fig. 8d), which confirmed the participation of $O_2^{\bullet-}$ in this reaction. However, BQ can also react with $HO^{\bullet}$ but the reaction is insignificant compared to $O_2^{\bullet-}$ [75]. Among used scavengers, the highest reduction in efficiency was observed in the presence of $HO^{\bullet}$ scavengers, which confirmed the dominant role of this species in COP.

Literature suggests that the ions including carbonate, phosphate, and sulfate have high affinity with the Lewis acids on the surface of catalyst [3]. Among these ions, phosphate ions showed the highest inhibition on the reaction efficiency due to their adsorption on the surface of the catalyst and their interaction with the hydroxyl groups through ligand exchange [76]. In the presence of phosphate ions, the reaction efficiency decreased from 100% to 81% that confirmed the role of the catalyst active sites in ozone decomposition and the formation of reactive species. These ions occupied the Lewis acid sites on the surface of catalyst, and affect the water adsorption on the surface of catalyst [77]. Also, by addition of carbonate the reaction efficiency was slightly decreased, which can be related to reaction of this ions with $HO^{\bullet}$, which leads to the formation of $CO_3^{\bullet-}$ radicals with lower oxidation potential and higher selectivity than $HO^{\bullet}$ (Eq. 17) [49].

$$HO^{\bullet} + CO_3^{2-} \rightarrow CO_3^{\bullet-} + HO^{-} \quad (17)$$

The presence of sulfate ions didn't have any effect on ACT degradation efficiency. This ion can scavenge the $HO^{\bullet}$ to generate sulfate radicals (Eq. 18), although this reaction is dependent on the pH values, and can only occur at strongly acidic media (pH < 3.0) [43]; here it seems rather uninvolved.

$$SO_4^{2-} + HO^{\bullet} \rightarrow SO_4^{\bullet-} + HO^{-} \quad pH < 3.0 \quad (18)$$

Based on the above results, four pathways are proposed for this reaction, which are summarized by the following equations (Eqs. 19–26). Firstly, the direct oxidation of ACT with O_3 can take place in the bulk (Eq. 19). Secondly, the ozone molecules can adsorb on the surface of the catalyst, and react with ACT molecules, which can lead to intermediates generation (Eq. 21). Furthermore, the ozone molecules can react with hydroxyl groups on the surface of catalyst (S) and produce $HO^{\bullet}$, and $O_2^{\bullet-}$. This reaction can occur on the surface of catalyst (Eqs. 23–26). It should be noted that the dissolved ozone has electrophilic characteristics. Therefore, the basic functional groups on the surface of catalyst have a critical role in transforming ozone molecules to $HO^{\bullet}$ species [72]. The presence of these basic functional groups was confirmed from the FT-IR (the broad peak at 3425 cm^{-1}), and XPS analysis. So, the –OH groups can accelerate ozone decomposition, and subsequently the formation of $HO^{\bullet}$.

1) *Direct oxidation of ACT with ozone molecules*

$$ACT + O_3 \rightarrow Intermediates + H_2O + CO_2 \quad (19)$$

2) *Oxidation of ACT with generated $HO^{\bullet}$ in the bulk solution*

$$ACT + HO^{\bullet} \rightarrow Intermediates + H_2O + CO_2 \quad (20)$$

3) *ACT oxidation via direct reaction of ACT with O_3 on the surface of catalyst*

$$S - O_3 + ACT \rightarrow Intermediates + H_2O + CO_2 \quad (21)$$

$$S - ACT + O_3 \rightarrow Intermediates + H_2O + CO_2 \quad (22)$$

4) *ACT oxidation by the generated radical under surface of catalyst*

$$S - OH + O_3 \rightarrow S - O_3^{\bullet} + HO^{\bullet} \quad (23)$$

$$S - O_3^{\bullet} \rightarrow S - O^{\bullet} + O_2 \quad (24)$$

$$S - O_3^{\bullet} + O_3 \rightarrow S + O_2^{\bullet -} + O_2 \quad (25)$$

$$S - ACT + HO^{\bullet}/O_2^{\bullet -} \rightarrow Intermediates \quad (26)$$

Based on the XRF results, the main oxides in C-HRS structure are α-Fe_2O_3 (57.95%), SiO_2 (18.72%), Al_2O_3 (3.82%), and CaO (3.78%). SiO_2 is not active in ozonation reactions and it is only used as support in COP [78,79]. Moreover, the metal oxides such as Al_2O_3 are not active in ozonation reaction, while the matrix pH is crucial [80]. CaO has been used in the ozonation reaction [81], but the CaO amount in our catalyst is very low. So, it has not critical role in this reaction. The main active oxide in C-HRS NPs is α-Fe_2O_3. The Lewis acid sites of catalyst (α-Fe_2O_3) have a great role in the formation of reactive species in the catalytic reaction. Based on the following equations (Eqs. 27–30), the chemisorbed O_3 was decomposed by the Lewis active sites of Fe^{3+} and produced the adsorbed hydroxyl radical ($HO^{\bullet}_{ads}$) and $HO_2^{\bullet}$ [75,82]. This reaction led to the reduction of Fe^{3+} to Fe^{2+} (Eq. 29). Due to the formation of hydrogen peroxide (H_2O_2) during these reactions and its subsequent reaction with and Fe^{2+}, the Fe^{3+} and $HO^{\bullet}$ are formed, that enhance the reaction efficiency (Eqs. 30 and 15). As discussed above, the following reactions have a role in formation of $HO^{\bullet}$ during the COP of ACT. Moreover, by addition of H_2O_2 solution into the reaction, more $HO^{\bullet}$ was generated via the reaction between O_3 and H_2O_2, as well as Fenton reaction (Eqs. 13–15). Fig. 11 illustrates the proposed mechanism of ACT degradation in C-HRS/O_3/H_2O_2 process.

$$\equiv Fe^{3+} + HO^{-} \rightarrow \equiv Fe^{3+} - OH \quad (27)$$

$$\equiv Fe^{3+} - OH + O_3 \rightarrow \equiv Fe^{3+} - O_3^{\bullet} + HO^{\bullet}_{ads} \quad (28)$$

$$\equiv Fe^{3+} - O_3^{\bullet} + HO^{-} \rightarrow \equiv Fe^{2+} + HO_2^{\bullet} + O_2 \quad (29)$$

$$2HO_2^{\bullet} \rightarrow H_2O_2 + O_2 \quad (30)$$

3.5. ACT degradation intermediates' identification by LC–MS analysis

In order to study the generated intermediates and by-products during the COP of ACT over C-HRS NPs, LC-MS analysis was applied, and the proposed degradation pathway was illustrated in Fig. 12. According to the results, ten main transformation products (TPs) were produced during this reaction based on their mass-to-charge (m/z) ratio. The O_3 molecules can attack the aromatic ring and produce two aromatic compounds (TP1, and TP2) and acetamide (TP3). In other AOPs-mediated treatment of ACT, hydroxylation is the main reaction in which the hydroxyl group was connected to the aromatic ring [47]. By the hydroxylation of ACT, 2-hydroxy-4-(N-acetyl) aminophenol (TP1) was produced. Moreover, two more products including hydroquinone (TP2), and acetamide (TP3) were obtained. Following, TP1 can oxidize to glycolic acid (TP6) as α-hydrogen acid. This compound was oxidized and converted to oxalic acid (TP7) and glyoxylic acid (TP8). Moreover, by the oxidation of TP2, 1, 4-benzoquinone (TP4) can be obtained. This compound can act as precursor for the formation of tartronic acid (TP9). Following, TP9 can be oxidized and converted to mesoxalic acid (TP10). Due to the presence of $HO^{\bullet}$ as main reactive species in this reaction, and the concurrent oxidation of intermediates, linear products were obtained, which were finally converted to H_2O and CO_2.

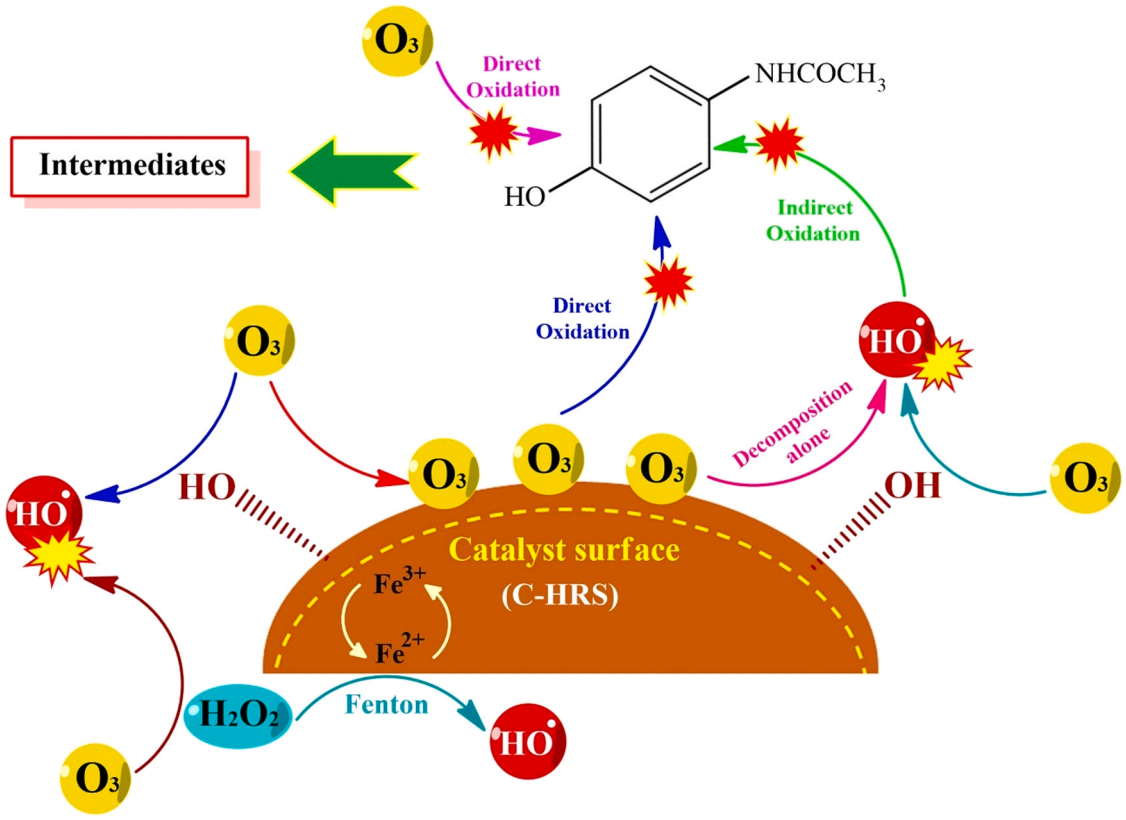

Fig. 11. Proposed catalytic ozonation process of ACT over C-HRS NPs.

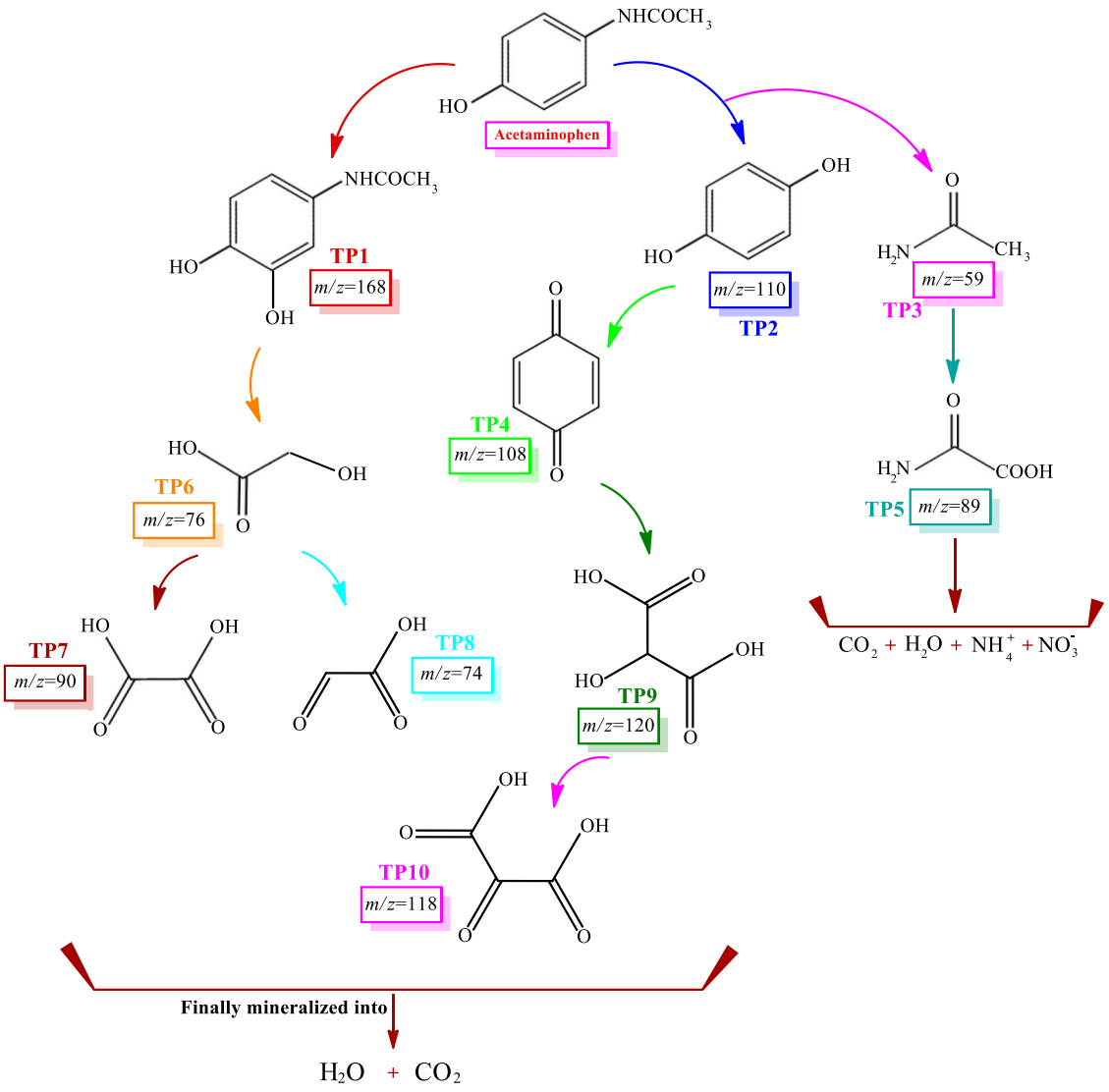

Fig. 12. Proposed pathway of ACT degradation over COP (Reaction conditions: [ACT] = 50 mg L^{-1}, [catalyst] = 1.0 g L^{-1}, pH = 7.0, [O_3] = 1.2 mg min^{-1}, and Reaction time = 30 min).

4. Conclusions

In this study, Hormuz Red Soil (HRS), a natural ferruginous soil, was used as an environmentally friendly catalyst in the catalytic ozonation of ACT with minor pre-treatment. After calcination at 600 °C, these C-HRS NPs exhibited high activity in degradation of ACT combined with ozone (C-HRS/O_3). The high activity of C-HRS was related to the structural modification of HRS during the calcination process, and the formation of oxygen vacancies as active catalytic sites. The reaction rate constant of catalytic ozonation process was 10.9 times higher than simple ozonation process that confirmed the vital role of C-HRS NPs in transforming of ozone to reactive species. Based on the results of our study, the highest activity was observed under basic conditions (pH > 7.0), due to the presence of more hydroxyl groups (-OH) that played the critical role in decomposition of ozone molecules, and the formation of hydroxyl radicals, but the process was adequately active at neutral pH as well. The catalytic activity of C-HRS was studied in enhancing the peroxone reaction (C-HRS/O_3/H_2O_2); C-HRS induced high ACT degradation and mineralization efficiency by assisting catalysis of peroxone. In this process, the Fe^{3+}/Fe^{2+} cycle and the synergy effects between O_3 and H_2O_2 can result in the formation of augmented *HO*• amounts. Based on the reactive species determination tests, surface-bound *HO*• played a critical role in ACT degradation mechanism. Finally, the catalyst was stable during five catalytic cycles (negligible leaching), without losing its activity nor being subject to changes in its crystalline structure and morphology. Considering the above, this natural catalyst can be used as precursor for the fabrication of hematite-based nanocomposites, specialized for advanced water treatment applications.

CRediT authorship contribution statement

Mona Kohantorabi: Investigation, Writing – original draft, Writing – review & editing, Visualization. Gholamreza Moussavi: Conceptualization, Methodology, Resources, Writing – original draft, Writing – review & editing, Supervision, Funding acquisition. Paula Oulego: Methodology, Validation, Visualization, Writing – review & editing. Stefanos Giannakis: Methodology, Validation, Visualization, Writing – original draft, Writing – review & editing, Supervision, Funding acquisition.

Declaration of Competing Interest

The authors declare that they have no known competing financial interests or personal relationships that could have appeared to influence the work reported in this paper.

Acknowledgment

This work was technically and financially supported by the Tarbiat Modares University, Iran, under the Research Group grant No. IG-39801. Stefanos Giannakis would like to acknowledge the Spanish Ministry of Science, Innovation and Universities (MICIU) for the Ramón y Cajal Fellowship (RYC2018-024033-I).

References

[1] M. Taghavi, M.T. Ghaneian, M.H. Ehrampoush, M. Tabatabaee, M. Afsharnia, A. Alami, J. Mardaneh, Feasibility of applying the LED-UV-induced TiO_2/ZnO-supported $H_3PMo_{12}O_{40}$ nanoparticles in photocatalytic degradation of aniline, Environ. Monit. Assess. 190 (2018) 188, https://doi.org/10.1007/s10661-018-6565-y.

[2] O. Nemati Sani, A.A. Navaei fezabady, M. Yazdani, M. Taghavi, Catalytic ozonation of ciprofloxacin using γ-Al_2O_3 nanoparticles in synthetic and real wastewaters, J. Water Process. Eng. 32 (2019), 100894, https://doi.org/10.1016/j.jwpe.2019.100894.

[3] A. Mashayekh-Salehi, G. Moussavi, K. Yaghmaeian, Preparation, characterization and catalytic activity of a novel mesoporous nanocrystalline MgO nanoparticle for ozonation of acetaminophen as an emerging water contaminant, Chem. Eng. J. 310 (2017) 157–169, https://doi.org/10.1016/j.cej.2016.10.096.

[4] C. Tan, N. Gao, Y. Deng, J. Deng, S. Zhou, J. Li, X. Xin, Radical induced degradation of acetaminophen with Fe_3O_4 magnetic nanoparticles as heterogeneous activator of peroxymonosulfate, J. Hazard. Mater. 276 (2014) 452–460, https://doi.org/10.1016/j.jhazmat.2014.05.068.

[5] G. Moussavi, Z. Hossaini, M. Pourakbar, High-rate adsorption of acetaminophen from the contaminated water onto double-oxidized graphene oxide, Chem. Eng. J. 287 (2016) 665–673, https://doi.org/10.1016/j.cej.2015.11.025.

[6] D.B. Silva, A. Cruz-Alcalde, C. Sans, J. Gimenez, S. Esplugas, Performance and kinetic modelling of photolytic and photocatalytic ozonation for enhanced micropollutants removal in municipal wastewaters, Appl. Catal. B: Environ. 249 (2019) 211–217, https://doi.org/10.1016/j.apcatb.2019.02.072.

[7] N. Fernandez-Saez, D.E. Villela-Martinez, F. Carrasco-Marin, A.F. Perez-Cadenas, L. M. Pastrana-Martinez, Heteroatom-doped graphene aerogels and carbon-magnetite catalysts for the heterogeneous electro-Fenton degradation of acetaminophen in aqueous solution, J. Catal. 378 (2019) 68–79, https://doi.org/10.1016/j.jcat.2019.08.020.

[8] A.G. Trovo, R.F.P. Nogueira, A. Aguera, A.R. Fernandez-Alba, S. Malato, Paracetamol degradation intermediates and toxicity during photo-Fenton treatment using different iron species, Water Res. 46 (2012) 5374–5380, https://doi.org/10.1016/j.watres.2012.07.015.

[9] F. Rashidashmagh, Y. Doekhi-Bennani, M. Tizghadam-Ghazani, J.P. van der Hoek, A. Mashayekh-Salehi, B.S.G.J. Heijman, K. Yaghmaeian, Synthesis and characterization of SnO_2 crystalline nanoparticles: a new approach for enhancing the catalytic ozonation of acetaminophen, J. Hazard. Mater. 404 (2021), 124154, https://doi.org/10.1016/j.jhazmat.2020.124154.

[10] J. Wang, H. Chen, Catalytic ozonation for water and wastewater treatment: recent advances and perspective, Sci. Total. Environ. 704 (2020), 135249, https://doi.org/10.1016/j.scitotenv.2019.135249.

[11] J. Marugán, J. Rodríguez-Chueca, S. Esplugas, C. Sans, S. Malato, Removal of pharmaceutically active compounds (PhACs) in wastewater by ozone and advanced oxidation processes. The Handbook of Environmental Chemistry, Springer,, Berlin, Heidelberg, 2020, https://doi.org/10.1007/698_2020_664.

[12] Y. Ku, W.J. Su, Y.S. Shen, Decomposition kinetics of ozone in aqueous solution, Ind. Eng. Chem. Res. 35 (1996) 3369–3374, https://doi.org/10.1021/ie9503959.

[13] J. Rivas, O. Gimeno, A. Encinas, F. Beltrán, Ozonation of the pharmaceutical compound ranitidine: reactivity and kinetic aspects, Chemosphere 76 (5) (2009) 651–656, https://doi.org/10.1016/j.chemosphere.2009.04.028.

[14] J.A. Malvestiti, A. Cruz-Alcalde, N. Lopez-Vinent, R.F. Dantas, C. Sans, Catalytic ozonation by metal ions for municipal wastewater disinfection and simulataneous micropollutants removal, Appl. Catal. B: Environ. 259 (2019), 118104 https://doi.org/10.106/j.apcatb.2019.118104.

[15] Y. Ling, G. Liao, P. Xu, L. Li, Fast mineralization of acetaminophen by highly dispersed Ag-g-C_3N_4 hybrid assisted photocatalytic ozonation, Sep. Purif. Technol. 216 (2019) 1–8, https://doi.org/10.1016/j.seppur.2019.01.057.

[16] N. Nasseh, F.S. Arghavan, S. Rudriguez-Coute, A.H. Panahi, M. Esmati, T.J. A-Musawi, Preparation of activated carbon@ZnO composite and its application as a novel catalyst in catalytic ozonation process for metronidazole degradation, Adv. Powder Technol. 31 (2) (2020) 875–885, https://doi.org/10.1016/j.apt.2019.12.006.

[17] A. Fischbacher, J. von Sonntag, C. von Sonntag, T.C. Schmidt, The •OH radical yield in the H_2O_2+O_3 (Peroxone) reaction, Environ. Sci. Technol. 47 (2013) 9959–9964, https://doi.org/10.1021/es402305r.

[18] I. Akmehmet Balcioglu, M. Otker, Treatment of pharmaceutical wastewater containing antibiotics by O_3 and O_3/H_2O_2 processes, Chemosphere 50 (2003) 85–95, http://doi.org/S0045-6535(02)00534-9.

[19] J.P. Pocostales, M.M. Sein, W. Knolle, C. von Sonntag, T.C. Schmidt, Degradation of ozone-refractory organic phosphates in wastewater by ozone and ozone/hydrogen peroxide (peroxone): the role of ozone consumption by dissolved organic matter, Environ. Sci. Technol. 44 (2010) 8248–8253, https://doi.org/10.1021/es1018288.

[20] Z. Guo, Y. Xie, J. Xiao, Z.J. Zhao, Y. Wang, Z. Xu, Y. Zhang, L. Yin, H. Cao, J. Gong, Single-atom Mn−N4 site-catalyzed peroxone reaction for the efficient production of hydroxyl radicals in an acidic solution, J. Am. Chem. Soc. 141 (2019) 12005–12010, https://doi.org/10.1021/jacs.9b04569.

[21] Z. Zeng, H. Zou, X. Li, B. Sun, J. Chen, L. Shao, Ozonation of acidic phenol wastewater with O_3/Fe(II) in a rotating packed bed reactor: optimization by response surface methodology, Chem. Eng. Process. Process. Intensif. 60 (2012) 1–8, https://doi.org/j.cep.2012.06.006.

[22] H. Zhang, Y. He, L. Lai, G. Yao, B. Lai, Catalytic ozonation of Bisphenol A in aqueous solution by Fe_3O_4–MnO_2 magnetic composites: performance, transformation pathways and mechanism, Sep. Purif. Technol. 245 (2020), 116449, https://doi.org/10.1016/j.seppur.2019.116449.

[23] A.G. Goncalves, J.L. Figueiredo, J.J.M. Orfao, M.F.R. Pereira, Influence of the surface chemistry of multi-walled carbon nanotubes on their activity as ozonation catalysts, Carbon 48 (2010) 4369–4381, https://doi.org/10.1016/j.carbon.2010.07.051.

[24] L. Zhou, S. Zhang, Z. Li, X. Liang, Z. Zhang, R. Liu, J. Yun, Efficient degradation of phenol in aqueous solution by catalytic ozonation over MgO/AC, J. Water Process. Eng. 36 (2020), 101168, https://doi.org/10.1016/j.jwpe.2020.101168.

[25] L. Yang, C. Hu, Y. Nie, J. Qu, Catalytic ozonation of selected pharmaceuticals over mesoporous alumina-supported manganese oxide, Environ. Sci. Technol. 43 (7) (2009) 2525–2529, https://doi.org/10.1021/es803253c.

[26] S. Sajjadi, A. Khataee, R.D.C. Soltani, A. Hasanzadeh, N, S co-doped graphene quantum dot–decorated Fe_3O_4 nanostructures: preparation, characterization and catalytic activity, J. Phys. Chem. Solid. 127 (2019) 140–150, https://doi.org/10.1016/j.jpcs.2018.12.014.

[27] J. Nowrocki, Catalytic ozonation in water: controversies and questions. Discussion paper, Appl. Catal. B: Environ. 142–143 (2013) 465–471, https://doi.org/10.1016/j.apcatb.2013.05.061.

[28] M. Zhang, D. Yin, J. Guo, H. Wu, M. Gong, X. Feng, Ternary catalyst Mn-Fe-Ce/Al_2O_3 for the ozonation of phenol pollutant: performance and mechanism, Environ. Sci. Pollut. Res (2021), https://doi.org/10.1007/s11356-021-13006-5.

[29] H. Zhao, Y. Dong, G. Wang, P. Jiang, J. Zhang, L. Wu, K. Li, Novel magnetically separable nanomaterials for heterogeneous catalytic ozonation of phenol pollutant: $NiFe_2O_4$ and their performances, Chem. Eng. J. 219 (2013) 295–302, https://doi.org/10.1016/j.cej.2013.01.019.

[30] P. Yan, J. Shen, L. Yuan, J. Kang, B. Wang, S. Zhao, Z. Chen, Catalytic ozonation by Si-doped α-Fe_2O_3 for the removal of nitrobenzene in aqueous solution, Sep. Pur. Technol. 228 (2019), 115766, https://doi.org/10.1016/j.seppur.2019.115766.

[31] A. Elfiad, F. Galli, A. Djadoum, M. Sennour, S. Chegrouche, L. Meddour-Boukhobza, D.C. Boffito, Natural α-Fe_2O_3 as an efficient catalyst for the p-nitrophenol reduction, Mater. Chem. Eng. B. 229 (2018) 126–134, https://doi.org/10.1016/j.mseb.2017.12.009.

[32] N. Basavegowda, K. Mishra, Y. Rok Lee, Synthesis, characterization, and catalytic applications of hematite (α-Fe_2O_3) nanoparticles as reusable nanocatalyst, Adv. Nat. Sci: Nanosci. Nanotechnol. 8 (2017), 025017, https://doi.org/10.1088/2043-6254/aa6885/meta.

[33] Z. Wei, R. Xing, X. Zhang, S. Liu, H. Yu, P. Li, Facile template-free fabrication of hollow nestlike α-Fe_2O_3 nanostructures for water treatment, ACS Appl. Mater. Interfaces 5 (2013) 598–604, https://doi.org/10.1021/am301950k.

[34] P.P. Sarangi, B. Naik, N.N. Ghosh, Low temperature synthesis of single-phase α-Fe_2O_3 nano-powders by using simple but novel chemical methods, Powder Technol. 192 (2009) 245–249, https://doi.org/10.1016/j.powtec.2009.01.002.

[35] M. Mohapatra, S. Anand, Synthesis and applications of nano-structured iron oxides/hydroxides – a review, Int. J. Eng. Sci. Technol. 2 (2010) 127–146, https://doi.org/10.4314/ijest.v2i8.63846.

[36] D. Xia, H. He, H. Liu, Y. Wang, Q. Zhang, Y. Li, A. Lu, C. He, P.K. Wong, Persulfate-mediated catalytic and photocatalytic bacterial inactivation by magnetic natural ilmenite, Appl. Catal. B: Environ. 238 (2018) 70–81, https://doi.org/10.1016/j.apcatb.2018.07.003.

[37] E. Expósito, C.M. Sánchez-Sánchez, V. Montiel, Mineral iron oxides as iron source in electro-Fenton and photoelectro-Fenton mineralization processes, J. Electrochem. Soc. 154 (2007) E116–E122, https://doi.org/10.1149/1.2744134/meta.

[38] R. Pelalak, R. Alizadeh, E. Ghareshabani, Enhanced heterogeneous catalytic ozonation of pharmaceutical pollutants using a novel nanostructure of iron-based mineral prepared via plasma technology: a comparative study, J. Hazard. Mater. 392 (2020), 122269, https://doi.org/10.1016/j.jhazmat.2020.122269.

[39] P. Kolosov, M.L. Peyot, V. Yargeau, Novel materials for catalytic ozonation of wastewater for disinfection and removal of micropollutants, Sci. Total. Environ. 644 (2018) 1207–1218, https://doi.org/10.1016/j.scitotenv.2018.07.022.

[40] S. Aredes, B. Klein, M. Pawlik, The removal of arsenic from water using natural iron oxide minerals, J. Clean. Prod. 60 (2013) 71–76, https://doi.org/10.1016/j.jclepro.2012.10.035.

[41] S. Mohammadi, G. Moussavi, S. Shekoohiyan, M.L. Marin, F. Bosca, S. Giannakis, A continuous-flow catalytic process with natural hematite-alginate beads for effective water decontamination and disinfection: peroxymonosulfate activation leading to dominant sulfate radical and minor non-radical pathways, Chem. Eng. J. 411 (2021), 127738, https://doi.org/10.1016/j.cej.2020.127738.

[42] M. Kohantorabi, S. Giannakis, M.R. Gholami, L. Feng, C. Pulgarin, A systematic investigation on the bactericidal transient species generated by photo-sensitization of natural organic matter (NOM) during solar and photo-Fenton disinfection of surface waters, Appl. Catal. B: Environ. 244 (2019) 983–995, https://doi.org/10.1016/j.apcatb.2018.12.012.

[43] M. Kohantorabi, G. Moussavi, P. Oulego, S. Giannakis, Radical-based degradation of sulfamethoxazole via UVA/PMS-assisted photocatalysis, driven by magnetically

separable Fe_3O_4@CeO_2@BiOI nanospheres, Sep. Purif. Technol. 267 (2021), 118665, https://doi.org/10.1016/j.seppur.2021.118665.
[44] M. Kohantorabi, S. Giannakis, G. Moussavi, M. Bensimon, M.R. Gholami, C. Pulgarin, An innovative, highly stable Ag/ZIF-67@GO nanocomposite with exceptional peroxymonosulfate (PMS) activation efficacy, for the destruction of chemical and microbiological contaminants under visible light, J. Hazard. Mater. 413 (2021), 125308, https://doi.org/10.1016/j.jhazmat.2021.125308.
[45] V. Shukla, Role of spin disorder in magnetic and EMI shielding properties of Fe_3O_4/C/PPy core/shell composites, J. Mater. Sci. 55 (7) (2020) 2826–2835, https://doi.org/10.1007/s10853-019-04198-w.
[46] J. Han, Y. Lai, Y. Xiang, S. Wu, Y. Xu, Y. Zeng, J. Chen, J. Liu, Glass structure of the CaO-B_2O_3-SiO_2-Al_2O_3-ZnO glasses systems with different Si content, J. Mater. Sci. 28 (2017) 6131–6137, https://doi.org/10.1007/s10854-016-6291-6.
[47] H. Salari, M. Kohantorabi, Fabrication of novel Fe_2O_3/MoO_3/AgBr nanocomposites with enhanced photocatalytic activity under visible light irradiation for organic pollutant degradation, Adv. Powder Technol. 31 (1) (2020) 493–503, https://doi.org/10.1016/j.apt.2019.11.005.
[48] H. Liu, T. Chen, X. Zou, C. Qing, R.L. Frost, Thermal treatment of natural goethite: thermal transformation and physical properties, Thermochim. Acta 568 (2013) 115–121, https://doi.org/10.1016/j.tca.2013.06.027.
[49] M. Kohantorabi, G. Moussavi, S. Mohammadi, P. Oulego, S. Giannakis, Photocatalytic activation of peroxymonosulfate (PMS) by novel mesoporous Ag/ZnO@$NiFe_2O_4$ nanorods, inducing radical-mediated acetaminophen degradation under UVA irradiation, Chemosphere 277 (2021), 130271, https://doi.org/10.1016/j.chemosphere.2021.130271.
[50] M. Elaref, W. Salama, R. Gaupp, Spectroscopic characterization of iron ores formed in different geological environments using FTIR, XPS, Mössbauer spectroscopy and thermoanalyses, Spectrochim. Acta A Mol. Biomol. Spectrosc. 136 (2015) 1816–1826, https://doi.org/10.1016/j.saa.2014.10.090.
[51] M.G. Syamala Rao, A. Sanchez-Martinez, G. Gutierrez-Heredio, M.A. Quevedo-Lopez, R. Ramirez-Bon, Sol-gel derived low temperature HfO_2-GPTMS hybrid gate dielectric for a-IGZO thin-film transistors (TFTs), Ceram. Inter. 44 (2018) 16428–16434, https://doi.org/10.1016/j.ceramint.2018.06.056.
[52] K.M. Eblagon, P.H. Concepción, H. Silva, A. Mendes, Ultraselective low temperature steam reforming of methanol over PdZn/ZnO catalysts—influence of induced support defects on catalytic performance, Appl. Catal. B: Environ. 154–155 (2014) 316–328, https://doi.org/10.1016/j.apcatb.2014.02.032.
[53] L. Wang, Y. Yu, H. He, Y. Zhang, X. Qin, B. Wang, Oxygen vacancy clusters essential for the catalytic activity of CeO_2 nanocubes for o-xylene oxidation, Sci. Rep. 7 (1) (2017) 1284, https://doi.org/10.1038/s41598-017-13178-6.
[54] Z. Wang, X. Mao, P. Chen, M. Xiao, S.A. Monny, S. Wang, M. Konarova, A. Du, L. Wang, Understanding the roles of oxygen vacancies in hematite-based photoelectrochemical processes, Angew. Chem. Int. Ed. 58 (4) (2019) 1030–1034, https://doi.org/10.1002/ange.201810583.
[55] P.L. Desbene, L. Silly, J.P. Morizur, M. Delamar, XPS analysis of humic and fulvic acids, Anal. Lett. 19 (21–22) (1986) 2131–2214, https://doi.org/10.1080/00032718608080871.
[56] S.D. Kalev, G.S. Toor, Chapter 3.9 - The composition of soils and sediments, in: B. Török, T. Dransfield (Eds.), Green Chemistry, Elsevier, 2018, pp. 339–357.
[57] N. Patel, I.R. Gibson, S. Ke, S.M. Best, W. Bonfield, Calcining influence on the powder properties of hydroxyapatite, J. Mater. Sci. Mater. Med 12 (2001) 181–188, https://doi.org/10.1023/A:1008986430940.
[58] J.L. Cao, Y. Wang, X.L. Yu, S.R. Wang, S.H. Wu, Z.Y. Yuan, Mesoporous CuO–Fe_2O_3 composite catalysts for low-temperature carbon monoxide oxidation, Appl. Catal. B Environ. 79 (2008) 26–34, https://doi.org/10.1016/j.apcatb.2007.10.005.
[59] S. Panigrahi, S. Basu, S. Praharaj, S. Pande, S. Jana, A. Pal, S.K. Ghosh, T. Pal, Synthesis and size-selective catalysis by supported gold nanoparticles: study on heterogeneous and homogeneous catalytic process, J. Phys. Chem. C. 111 (2007) 4596–4605, https://doi.org/10.1021/jp067554u.
[60] L. Lei, D. Huang, G. Zeng, M. Cheng, D. Jiang, C. Zhou, S. Chen, W. Wang, A fantastic two-dimensional MoS_2 material based on the inert basal planes activation: Electronic structure, synthesis strategies, catalytic active sites, catalytic and electronics properties, Coord. Chem. Rev. 399 (2019), 213020, https://doi.org/10.1016/j.ccr.2019.213020.
[61] B. Kasprzyk-Hordern, M. Ziółek, J. Nawrocki, Catalytic ozonation and methods of enhancing molecular ozone reactions in water treatment, Appl. Catal. B: Environ. 4 (2003) 639–669, https://doi.org/10.1016/S0926-3373(03)00326-6.
[62] K. Yaghmaeian, G. Moussavi, A. Mashayekh-Salehi, A. Mohseni-Bandpei, M. Satari, Oxidation of acetaminophen in the ozonation process catalyzed with modified MgO nanoparticles: effect of operational variables and cytotoxicity assessment, Process. Saf. Environ. Prot. 109 (2017) 520–528, https://doi.org/10.1016/j.psep.2017.04.020.
[63] B. Wang, H. Zhang, F. Wang, X. Xiong, F. Wang, X. Xiong, K. Tian, Y. Sun, T. Yu, Application of heterogeneous catalytic ozonation for refractory organics in wastewater, Catalysts 9 (3) (2019) 241, https://doi.org/10.3390/catal9030241.
[64] Y.H. Han, K. Ichikawa, H.A. Utsumi, Kinetic study of enhancing effect by phenolic compounds on the hydroxyl radical generation during ozonation, Water Sci. Technol. 5 (2004) 97–102, https://doi.org/10.2166/wst.2004.0497.
[65] F.J. Beltran. Ozone Reaction Kinetics for Water and Wastewater Systems, Lewis Publications,, Boca Raton, FL, 2004.
[66] O. Lorphensri, J. Intravijit, D.A. Sabatini, T.C.G. Kibbey, K. Osathaphan, C. Saiwan, Sorption of acetaminophen, 17α-ethyl estradiol, nalidixic acid, and norfloxacin to cilica, alumina, and a hydrophobic medium, Water Res. 40 (2006) 1481–1491, https://doi.org/10.1016/j.watres.2006.02.003.
[67] M. Neamtu, M. Bobu, A. Kettrup, I. Siminiceanu, Ozone photolysis of paracetamol in aqueous solution, J. Environ. Sci. Health 48 (2013) 1264–1271, https://doi.org/10.1080/10934529.2013.776898.
[68] J. Singh, S. Sharma, S. Aanchal, Basu, Synthesis of Fe_2O_3/TiO_2 monoliths for the enhanced degradation of industrial dye and pesticide via photo-Fenton catalysis, J. Photochem. Photobiol. A: Chem. 376 (2019) 32–42, https://doi.org/10.1016/j.jphotochem.2019.03.004.
[69] J. Xie, X. Li, W. Chen, X. Sun, K. Chen, Y. Tang, L. Li, Enhanced mineralization of oxalate by heterogeneous peroxone: the interfacial reaction on the core-shell CeO_x@SiO_2, Chem. Eng. J. 379 (2020), 122344, https://doi.org/10.1016/j.cej.2019.122344.
[70] R. Li, Y. Huang, D. Zhu, W. Ho, J. Cao, S. Lee, Improved oxygen activation over a carbon/Co_3O_4 nanocomposite for efficient catalytic oxidation of formaldehyde at room temperature, Environ. Sci. Technol. 55 (6) (2021) 4054–4063, https://doi.org/10.1021/acs.est.1c00490.
[71] E. Brillas, I. Sirés, M.A. Oturan, Electro-Fenton process and related electrochemical technologies based on Fenton's reaction chemistry, Chem. Rev. 109 (2009) 6570–6631, https://doi.org/10.1021/cr900136g.
[72] M. Kohantorabi, G. Moussavi, S. Giannakis, A review of the innovations in metal- and carbon-based catalysts explored for heterogeneous peroxymonosulfate (PMS) activation, with focus on radical vs. non-radical degradation pathways of organic contaminants, Chem. Eng. J. 411 (2021), 127957, https://doi.org/10.1016/j.cej.2020.127957.
[73] F. Rashidashmagh, Y. Doekhi-Bennani, M. Tizghadam-Ghazani, J.P.V. der Hoek, A. Mashayekh-Salehi, B.S.G.J. Heijman, K. Yaghmaeian, Synthesis and characterization of SnO_2 crystalline nanoparticles: a new approach for enhancing the catalytic ozonation of acetaminophen, J. Hazard. Mater. 404 (2021), 124154, https://doi.org/10.1016/j.jhazmat.2020.124154.
[74] L. Yang, L.E. Yu, M.B. Ray, Photocatalytic oxidation of paracetamol: dominant reactants, intermediates, and reaction mechanisms, Environ. Sci. Technol. 43 (2009) 460–465, https://doi.org/10.1021/es8020099.
[75] N. Jaafarzadeh, F. Ghanbari, M. Ahmadi, Efficient degradation of 2,4-dichlorophenoxyacetic acid by peroxymonosulfate/magnetic copper ferrite nanoparticles/ozone: a novel combination of advanced oxidation processes, Chem. Eng. J. 320 (2017) 436–447, https://doi.org/10.1016/j.cej.2017.03.036.
[76] T. Zhang, J. Ma, Catalytic ozonation of trace nitrobenzene in water with synthetic goethite, J. Mol. Catal. Chem. 279 (2008) 82–89, https://doi.org/10.1016/j.molcata.2007.09.030.
[77] A. Lv, C. Hu, Y. Nie, J. Qu, Catalytic ozonation of toxic pollutants over magnetic cobalt and manganese co-doped γ-Fe_2O_3, Appl. Catal. B Environ. 100 (2010) 62–67, https://doi.org/10.1016/j.apcatb.2010.07.011.
[78] P.F. Biard, B. Werghi, I. Soutrel, R. Orhand, A. Couvert, A. Denicourt-Nowicki, A. Roucoux, Efficient catalytic ozonation by ruthenium nanoparticles supported on SiO_2 or TiO_2: towards the use of a non-woven fiber paper as original support, Chem. Eng. J. 289 (2016) 374–381, https://doi.org/10.1016/j.cej.2015.12.051.
[79] W. Chen, J. Xie, X. Li, L. Li, Oxygen vacancies and Lewis sites activating O_3/H_2O_2 at wide pH range via surface electron transfer over CeO_x@SiO_2 for nitrobenzene mineralization, J. Hazard. Mater. 406 (2021), 124760, https://doi.org/10.1016/j.jhazmat.2020.124766.
[80] J. Nawrocki, L. Fijołek, Effect of aluminium oxide contaminants on the process of ozone decomposition in water, Appl. Catal. B: Environ. 142–143 (2013) 533–537, https://doi.org/10.1016/j.apcatb.2013.05.069.
[81] J. Wu, T. Su, Y. Jiang, X. Xie, Z. Qin, H. Ji, Catalytic ozonation of cinnamaldehyde to benzaldehyde over CaO: experiments and intrinsic kinetics, AIChE J. 63 (10) (2017) 4403–4417, https://doi.org/10.1002/aic.15773.
[82] L. Lei, D. Huang, C. Zhou, S. Chen, X. Yan, Z. Li, W. Wang, Demystifying the active roles of NiFe-based oxides/(oxy)hydroxides for electrochemical water splitting under alkaline conditions, Coord. Chem. Rev. 408 (2020), 213177, https://doi.org/10.1016/j.ccr.2019.213177.